Scattering of NO from Au(111)
- A Quantum Dissipative Study -

Inaugural-Dissertation

to obtain the academic degree
Doctor rerum naturalium (Dr. rer. nat.)

submitted to
the Department of Biology, Chemistry and Pharmacy
of Freie Universität Berlin

by

Tobias Serwatka

March 2020

This work was prepared under supervision of

Prof. Jean Christophe Tremblay, Ph.D.
(CNRS/Université de Lorraine)
from
April 2017 until March 2020

First Reviewer:	Prof. Jean Christophe Tremblay, Ph.D.
Second Reviewer:	Prof. Dr. Beate Paulus
Date of Defense:	May 27$^{\text{th}}$, 2020

"*Dans la vie, rien n'est à craindre, tout est à comprendre.*"
attributed to Marie Curie (1867-1934)

Abstract

The energy transfer between surfaces and adsorbates is a key aspect to gain a deeper insight into many processes at surfaces, such as dissociation, adsorption and others which are important in heterogeneous catalysis. The purpose of this thesis is to provide a better understanding of the energy transfer between adsorbate vibrations and electron-hole pairs for the scattering of NO from a Au(111) surface. In the first part of this dissertation the NO/Au(111) system is described in static terms. A new six-dimensional representation of the potential energy surface of the adiabatic ground state is constructed based on elecronic structure calculations in a density functional theory framework. This representation employs a site-based strategy that rests upon a global, physically-motivated, analytic form which is able to account for a partial charge transfer between surface and adsorbate. The system is spectroscopically characterized by the anharmonic eigenstates of the constructed potential energy surface. These full-dimensional vibrational eigenstates reveal a distinct coupling between the system modes, especially between the tilt angle and the molecule-surface distance.
In the second part of this thesis a wave function based quantum dynamical model in reduced dimensions is developed. It employs a stochastic propagator that accounts for the coupling of molecular vibrations to electron-hole pairs of the surface by a specially designed relaxation basis. That basis guides the wave packet towards the surface during quantum jumps induced by the system's excitonic environment. The associated anharmonic transition rates are obtained from first-order perturbation theory. These rates are ensured to vanish asymptotically reflecting the evanescent coupling strength far away from the surface. Test calculations for the NO/Au(111) system show the favourable convergence behaviour of the model as well as its ability to capture typical processes on metal surfaces, such as trapping or vibrational relaxation.
Finally, the developed potential energy surface and the quantum dynamical model are utilized to study the scattering of NO($\nu = 3$) from Au(111) in detail. It is demonstrated for the first time that by considering the coupling to electron-hole pairs the experimentally observed trend of increasing relaxation probability as a function of the initial kinetic energy can be qualitatively reproduced. Additionally, the energy transfer between the different modes is analyzed showing a strong redistribution from translation to rotations leading to rotationally highly excited states. The translational mode is also found to be of major importance for the energy transfer between molecule and surface. The comparison between classical and quantum dynamical simulations shows the former to yield wrong trends compared to experiment. That emphasizes the importance of quantized relaxation in the scattering dynamics of NO from Au(111).

Kurzzusammenfassung

Der Energieaustausch zwischen Oberflächen und Adsorbaten ist ein zentraler Aspekt um tiefere Einblicke in zahlreiche Prozesse auf Oberflächen zu erhalten, wie z.B. Dissoziation, Adsorption und weitere Prozesse mit besonderer Relevanz für heterogene Katalyse. Das Ziel dieser Arbeit ist es ein besseres Verständnis für den Energieaustausch zwischen Adsorbatschwingungen und Elektron-Loch-Paaren während der Streuung von NO auf Au(111) zu erlangen. Im ersten Teil dieser Dissertation werden die statischen Eigenschaften des NO/Au(111)-Systems beschrieben. Für den adiabatischen Grundzustand wird eine neue Darstellung der Potentialenergiefläche in sechs Dimensionen konstruiert, welche auf Dichtefunktional-basierten Elektronenstrukturrechnungen fußt. Für diese Darstellung wird ein Adsorptionsstellen-basierter Ansatz gewählt, welcher auf einer globalen, physikalisch motivierten, analytischen Form beruht, die in der Lage ist den teilweisen Ladungstransfer zwischen Oberfläche und Adsorbat zu berücksichtigen. Mit Hilfe der anharmonischen Eigenzustände der erstellten Potentialenergiefläche wird das System charakterisiert. Diese sechsdimensionalen Schwingungseigenzustände offenbaren eine ausgeprägte Kopplung zwischen den Moden des Systems, insbesondere zwischen dem Kippwinkel und dem Abstand des Moleküls zur Oberfläche.
Im zweiten Teil dieser Arbeit wird ein quantendynamisches Modell in reduzierten Dimensionen entwickelt, das auf einer Beschreibung mittels Wellenfunktionen beruht. Dabei wird ein stochastischer Propagator verwendet, der die Kopplung der Molekülschwingungen und Elektron-Loch-Paare mit Hilfe einer speziellen Relaxationsbasis berücksichtigt. Bei Quantensprüngen, welche durch die exzitonische Umgebung induziert werden, lenkt diese Basis das Wellenpacket in Richtung der Oberfläche. Die dazugehörigen anharmonischen Übergangsraten werden mit Hilfe von Störungsrechnung erster Ordnung erhalten. Es ist gewährleistet, dass diese Raten asymptotisch verschwinden und damit die verschwindende Kopplungsstärke weit weg von der Oberfläche modellieren. In Testrechnungen wird das vorteilhafte Konvergenzverhalten des Modells gezeigt, sowie seine Fähigkeit typische Oberflächenprozesse wie Trapping oder Schwingungsrelaxation zu beschreiben.
Zum Abschluss werden die Potentialenergiefläche und das Quantenmodell verwendet, um die Streuung von NO($\nu = 3$) auf Au(111) detailliert zu untersuchen. Es wird zum ersten Mal gezeigt, dass der experimentelle Trend der steigenden Relaxationswahrscheinlichkeit als Funktion der kinetischen Anfangsenergie qualitativ reproduziert werden kann, wenn die Kopplung zu Elektron-Loch-Paaren berücksichtigt wird. Zusätzlich wird der Energieaustausch zwischen den Moden analysiert, bei welchem eine deutliche Umverteilung von Translation zu Rotationen beobachtet wird, die zu hoch angeregten Rotationszuständen führt. Des Weiteren zeigt es

sich, dass die Translationsmode von großer Bedeutung für den Energieaustausch zwischen Molekül und Oberfläche ist. Der Vergleich zwischen klassischen und quantendynamischen Simulationen zeigt, dass erstere falsche Trends produzieren. Dies unterstreicht die Bedeutung der quantisierten Relaxation für die Streudynamik von NO auf Au(111).

Contents

List of Publications

Paper A T. Serwatka, B. Paulus and J. C. Tremblay
"A new six-dimensional potential energy surface for NO/Au(111)"
Mol. Phys. **117**, 42–57 (2019)
DOI: 10.1080/00268976.2018.1492041

Paper B T. Serwatka and J. C. Tremblay
"Stochastic wave packet approach to nonadiabatic scattering of diatomic molecules from metals"
J. Chem. Phys. **150**, 184105 (2019)
DOI: 10.1063/1.5092698

Paper C T. Serwatka, G. Füchsel and J. C. Tremblay
"Scattering of NO(ν=3) from Au(111): a stochastic dissipative quantum dynamical perspective"
Phys. Chem. Chem. Phys. (2020), Advance Article
DOI: 10.1039/C9CP06084G

List of Figures

List of Abbreviations

CAP	Complex absorbing potential
CASSCF	Complete active space self-consistent field
CASPT2	Complete active space second-order perturbation theory
CISD	Configuration interaction singles and doubles
DFT	Density functional theory
Dtm	Deterministic
GGA	Generalized gradient approximation
HF	Hartree-Fock
IMC	Intermode coupling
LDA	Local-density approximation
LDFA	Local-density friction approximation
MCTDH	Multiconfigurational Time-Dependendent Hartree
MDEF	Molecular dynamics with electronic friction
MO-LCAO	Molecular orbitals as linear combination of atomic orbitals
PES	Potential energy surface
PDP	Piecewise deterministic process
QD	Quantum dynamics
VDOS	Vibrational density of states

Chapter 1

Introduction

Heterogeneous catalysis is a central process in many chemical reactions ranging from industrial syntheses (Haber-Bosch process,[1–3] Fischer-Tropsch process[4–6]) to electrochemical reactions.[7–9] A microscopic understanding of the relevant processes is essential to design and control these catalytic reactions. Due to their good controllability small molecules like CO, NO, NH_3 or CH_4[10] are used as model systems to yield a deeper insight into relevant aspects of catalytic processes. Of special interest is the energy transfer between the adsorbate vibrations and the surface degrees of freedom which often plays an important role in diffusion, trapping, dissociation, adsorption, and desorption processes.[11] In these the surface acts as a reservoir which transfers energy to and absorbs energy from the adsorbate, respectively.[12] For many systems there are two main mechanisms describing how the energy transfer proceeds. The first involves the coupling of the adsorbate vibrations to surface phonons and is typically found in semiconductors and insulators for which the vibrational energy lies in the band gap.[13–16] It is also observed for low-frequency modes at metals, e.g. in the inelastic scattering of NH_3 from Au(111),[17] the desorption of CO from Ru(0001),[18,19] the dissociative chemisorption of N_2 on Ru(0001)[20] or the scattering of HCl from Au(111) at low temperatures.[21,22] In metals, the missing band gap offers a second energy exchange mechanism: the coupling of molecular vibrations to electron-hole pairs of the surface.[23–28] This was first reported for the scattering of NO from Ag(111)[29,30] and was since discovered for many more processes and systems like inelastic scattering of diatomic molecules from metals,[22,31–34] adsorption of hydrogen on metal surfaces,[35–41] chemicurrents[42–45] or vibrational promotion of electron emission.[46–50] The coupling to electron-hole pairs also results in vibrational lifetimes in the picosecond regime,[51–57] e.g. for CO on Cu(100) where a vibrational lifetime of 2 ± 1 ps[53] was observed compared to phonon-induced lifetimes in the microsecond regime found for CO on NaCl.[58]

The scattering of NO from a gold (111) surface is perhaps one of the most prominent and extensively studied systems for which an electron-mediated energy trans-

fer is supposed. In 2000 Huang *et al.* observed for the scattering of NO($\nu = 15$) from Au(111) a significant redistribution of vibrational states leading to a broadening and a shift of seven to eight quanta, which corresponds to an energy loss of $\sim$150 kJ mol^{-1}.[59] They attributed this vibrational relaxation mainly to electron-hole pairs since only a small relaxation was found in comparable scattering experiments on an insulating LiF(001) surface. Besides, the relaxation on Au(111) proceeds on a rather short time scale in the sub-picosecond regime which is too short for typical phonon-mediated processes. Further indications for nonadiabaticity of the NO/Au(111) system were found in studies of the excitation probability for NO($\nu = 0$). In these studies an Arrhenius-like temperature dependence shows an activated process with an activation energy on the scale of the vibrational energies.[60–62] In contrast, phonon-mediated excitations are often weakly affected by temperature[17,22] or have an activation energy dependent on the initial energy.[63,64] An increase in initial translational energy increases the excitation probability but the missing energy threshold excludes internal energy conversion as an excitation channel. The scattering of NO($\nu = 3$) reveals the same trend for the relaxation probabilities,[65] as well as a strong orientational dependence of these probabilities. When the molecules are oriented with the O atom pointing to the surface the relaxation probabilities are strongly diminished.[66,67] In addition, the Au(111) surface was shown to act as an energy reservoir to which a significant amount of translational energy of the molecule is transferred.[12]

The theoretical description of the mentioned transfer mechanisms can be a complicated task, especially for the electron-mediated coupling. For the vibration-phonon coupling it is comparatively straightforward since it only requires a potential energy surface (PES) in the adiabatic ground state. Based on this, due to the large masses and the approximately harmonic behaviour of the surface atoms, the dynamics is typically described in a classical fashion, where the motion of surface atoms can be included either explicitly[20,68–70] or implicitly by generalized Langevin oscillators.[71–75] By using the Multiconfigurational Time-Dependent Hartree (MCTDH) method[76] it is even feasible to perform quantum simulations. In contrast to phonon-mediated processes, the correct description of electron-mediated dynamics on surfaces is a much more challenging task since the excitation of electron-hole pairs creates electronically excited states and thus violates the Born-Oppenheimer approximation.[24,28] Therefore it is necessary to go beyond an adiabatic description. That is typically done by considering two limiting cases: the strong coupling and the weak coupling limits.[77] In the former an excited state which is of different character than the ground state is explicitly included in the description. That can be done by using model systems[77–80] or by calculating *ab initio* potential energy surfaces. The dynamical description is usually performed by classical hopping sim-

ulations.[81–83] However, even though it is by now possible to calculate excited states rather accurately, as shown e.g. for H_2 on Au[84,85] and CO on Cu(111)[86] by using embedded cluster models,[87–90] it is still a challenging task to obtain a complete PES in many dimensions. The second limiting case does not require an explicit inclusion of the excited state since in the weak coupling limit it is assumed that the state's character stays the same during the electronic excitation. If the nuclei are described classically, the electronic excitations lead to a frictional force acting on the system which moves on the adiabatic ground state PES.[91–93] If the nuclei are described quantum mechanically the coupling to the electron-hole pairs induces transitions between the molecule's vibrational states described by transition rates reflecting the strength of the coupling.[94]
Such a quantum mechanical description is employed in **Paper B**. In this paper a quantum dynamical model is constructed which describes the scattering of a diatomic molecule from a metal surface in reduced dimensions. The time evolution is based on a stochastic propagator including anharmonic transition rates and specially designed relaxation operators which describe the effect of the excitonic environment on the system states.

Over the last twenty years, the inelastic scattering of vibrationally excited NO from Au(111) was investigated by classical as well as quantum mechanical approaches in order to assess the importance of vibrational coupling to electron-hole pairs. In a Monte-Carlo wave packet approach based on a semiempirical two-state model in two dimensions Li and Guo could demonstrate the electron-mediated process to be capable of explaining the experimental findings qualitatively.[79] These qualitative findings were also confirmed by Shenvi *et al.* performing a kinetic study by means of a Pauli master equation.[80] Tully and coworkers constructed a diabatic two-state model in six dimensions from density functional theory (DFT) calculations. On these surfaces they performed surface hopping as well as molecular dynamics with electronic friction (MDEF) simulations for several initial conditions.[62,65,95–98] They found a shift and a broadening of the vibrational distribution for highly excited NO ($\nu = 11$, $\nu = 15$) but it was significantly smaller than observed in experiment.[98] In a study of inelastic scattering of NO($\nu = 3$) with different initial kinetic energies they could not reproduce the experimental trend of increasing relaxation probability as a function of these energies. Krüger *et al.* claimed the experimental and theoretical differences to be caused by inaccuracies of the PES.[98] In their model the NO molecule stays on the surface too long contradicting the experimentally observed direct scattering.[59] Only if trajectories that undergo multiple bounces are deselected they can provide the correct trend.
For that reason a new adiabatic representation of the six-dimensional PES is con-

structed in **Paper A**. It provides a global description of the potential energy landscape by using physically-motivated potential terms. That ensures a correct characterization of the asymptotic region of the configurational space. Furthermore, it diminishes the number of required fitting points without the occurence of underfitting issues. In contrast to the PES of Roy *et al.*[95] it also contains the top site of the (111) surface.
The issue of an accurate adiabatic PES was recently adressed by Yin *et al.* who included the surface atoms to construct a high-dimensional PES. Their work, which was done in parallel to the study in **Paper A**, demonstrates that the explicit consideration of phonons can reproduce the experimental trends for NO($\nu = 3$) in a classical simulation without including coupling to electron-hole pairs.[99] However, there is still a discrepancy between the theoretical results and the experimental findings which leaves the question about the importance of coupling to electron-hole pairs still open. A quantum dynamical study only based on electron-hole pair coupling was performed by Monturet and Saalfrank. They employed the coupled-channel density matrix method for NO($\nu = 15$) by considering only two dimensions (the bond length r, and the molecule-surface distance z).[100] Quantized vibrational relaxations were only considered along r with z-dependent harmonic transition rates. Monturet and Saalfrank could show a broadening of the vibrational distribution and a shift to lower-lying states but as in previous studies the obtained shift was too small.

It is still an open question how important the coupling to electron-hole pairs is to describe the trends for scattering of NO($\nu = 3$) from Au(111) and how important a quantum dynamical treatment is. Therefore a detailed study of the scattering process is performed in **Paper C** where the four-dimensional quantum model developed in **Paper B** is employed. Additionally, the quantum simulations are compared to classical simulations. That is done to adress the importance of quantized relaxations and to investigate how justified the application of classical methods in previous studies[98,99] is.

This thesis is organised as follows: Chapter 2 offers an overview of the theoretical models and approaches which were employed in this thesis. It begins with a brief introduction to the Schrödinger equation, its formulation in different pictures and the Born-Oppenheimer approximation in Sec. 2.1. The following section covers a short presentation of the Hartree-Fock method, density functional theory and the general description of periodic systems. In Sec. 2.3 the derivation of the quantum master equation in the weak coupling limit and its unravelling by a piecewise deterministic process (PDP) is reviewed. Besides, the coupling of molecular vibrations to electron-hole pairs within a classical friction framework and a quantum mechanical

perturbative treatment is discussed. That is followed by Chapter 3 which summarizes and discusses the central results of the publications listed in Chapter 4.

Chapter 2

Theory

2.1 Basic principles

This section will deal with some fundamental aspects of quantum mechanics. At first, the time-dependent Schrödinger equation and its alternative formulations will be introduced and explained. Afterwards, the separation of electronic and nuclear wave functions by the Born-Oppenheimer approximation will be presented. If not stated otherwise the textbooks of Tannor[101] and Nolting[102] were used as references. Apart from Sec. 2.3.4 atomic units will be employed in the complete chapter.

2.1.1 Schrödinger equation and quantum mechanical pictures

In non-relativistic quantum mechanics, the time-dependent Schrödinger equation[103]

$$i\frac{\partial}{\partial t}\Psi(\vec{Q},t) = \hat{H}\Psi(\vec{Q},t) \tag{2.1}$$

is the central equation of motion. It describes the evolution of a system characterized by its wave function $\Psi(\vec{Q},t)$. The Hamilton operator $\hat{H}$ in Eq. (2.1) defines the system's constituents and its interactions. In general, the Hamiltonian as well as the wave function depend on the time t and the non-temporal degrees of freedom $\vec{Q}$. However, there are systems whose Hamiltonians are not explicitely time-dependent, making it possible to employ a product ansatz for the wave function and simplifying Eq. (2.1) to the time-independent Schrödinger equation,

$$\hat{H}\Phi(\vec{Q}) = E\Phi(\vec{Q}). \tag{2.2}$$

The total wave function can be expressed as a product of a time-dependent part and the solution of Eq. (2.2), i.e. $\Psi(\vec{Q},t) = e^{-iEt}\Phi(\vec{Q})$, where the time-dependent

part is just a phase factor determined by the energy eigenvalue E.
In the formalism of Eq. (2.1) it is assumed that the wave function $\Psi(\vec{Q},t) = |\Psi(t)\rangle$ is time-dependent and the operators $\hat{A}$ are at most explicitely time-dependent. This so-called Schrödinger picture is the most common way to describe the evolution of quantum mechanical systems, but it is not the only one. A different approach represents the Heisenberg picture, in which the operators $\hat{A}_{\mathrm{H}}$ are time-dependent and linked to the operators $\hat{A}$ in the Schrödinger picture by

$$\hat{A}_{\mathrm{H}} = e^{i\hat{H}t}\hat{A}e^{-i\hat{H}t}. \tag{2.3}$$

Based on Eq. (2.3) it is possible to define an equation of motion of the operators

$$\frac{\mathrm{d}}{\mathrm{d}t}\hat{A}_{\mathrm{H}} = i\left[\hat{H}_{\mathrm{H}}, \hat{A}_{\mathrm{H}}\right] + \frac{\partial}{\partial t}\hat{A}_{\mathrm{H}}. \tag{2.4}$$

In contrast to the Schrödinger picture, the wave function in the Heisenberg picture is time-independent

$$|\Psi(t)\rangle_{\mathrm{H}} = e^{i\hat{H}t}\,|\Psi(t)\rangle = |\Psi(0)\rangle\,. \tag{2.5}$$

There is a third representation, the Dirac or interaction picture. Here, both the wave function $|\Psi(t)\rangle_{\mathrm{I}}$ as well as the operators $\hat{A}_{\mathrm{I}}(t)$ contain parts of the time evolution. They are defined as

$$|\Psi(t)\rangle_{\mathrm{I}} = e^{i\hat{H}_0 t}\,|\Psi(t)\rangle \tag{2.6}$$

and

$$\hat{A}_{\mathrm{I}}(t) = e^{i\hat{H}_0 t}\hat{A}(t)e^{-i\hat{H}_0 t} \tag{2.7}$$

for a system whose Hamiltonian is

$$\hat{H} = \hat{H}_0 + \hat{V}(t). \tag{2.8}$$

The corresponding equations of motion are

$$i\frac{\partial}{\partial t}\,|\Psi(t)\rangle_{\mathrm{I}} = \hat{V}_{\mathrm{I}}(t)\,|\Psi(t)\rangle_{\mathrm{I}} \tag{2.9}$$

and

$$\frac{\mathrm{d}}{\mathrm{d}t}\hat{A}_{\mathrm{I}}(t) = i\left[\hat{H}_0, \hat{A}_{\mathrm{I}}(t)\right] + \frac{\partial}{\partial t}\hat{A}_{\mathrm{I}}(t). \tag{2.10}$$

All three representation are physically equivalent, i.e. they all yield the same expectation values.

2.1.2 Born-Oppenheimer approximation

In quantum chemistry a Hamiltonian of a field-free molecular system with N electrons and M nuclei can be written as

$$\begin{aligned}\hat{H} =& -\sum_{i=1}^{N}\frac{1}{2}\Delta_i + \sum_{i=1}^{N}\sum_{j>i}^{N}\frac{1}{|\vec{r}_i-\vec{r}_j|} - \sum_{\alpha=1}^{M}\sum_{i=1}^{N}\frac{Z_\alpha}{|\vec{R}_\alpha-\vec{r}_i|} + \sum_{\alpha=1}^{M}\sum_{\beta>\alpha}^{M}\frac{Z_\alpha Z_\beta}{|\vec{R}_\alpha-\vec{R}_\beta|} \\ & -\sum_{\alpha=1}^{M}\frac{1}{2M_\alpha}\Delta_\alpha \qquad (2.11)\\ =& \hat{T}_\mathrm{e}+\hat{V}_\mathrm{ee}+\hat{V}_\mathrm{eN}+\hat{V}_\mathrm{NN}+\hat{T}_\mathrm{N}, \qquad (2.12)\end{aligned}$$

where M_α denotes the mass of nucleus α and Z_α its charge. The Hamiltonian consists of the kinetic operators ($\hat{T}$) of nuclei (N) and electrons (e) as well as the potential operators ($\hat{V}$) describing their interactions.
For a many-particle system (electrons as well as nuclei) Eq. (2.2) cannot be solved analytically and even numerical treatment might be quite difficult due to the coupling between both the electronic and the nuclear degrees of freedom, $\{\vec{r}_i\}$ and $\{\vec{R}_\alpha\}$. To circumvent this issue, the coupling between the electronic and nuclear degrees of freedom is neglected by employing the Born-Oppenheimer approximation.[104] It permits the successive evaluation of first the electronic and second the nuclear wave function.
The starting points for that approach is the large mass ratio between the nuclei and the electrons, resulting in different time scales of motion for both species. From the electrons' perspective the nuclei stay at rest and the electrons instantaneously adjust to the changing nuclear configuration. Therefore, in the first step of the Born-Oppenheimer approximation the Hamiltonian in Eq. (2.12) is separated in an electronic part $\hat{H}_\mathrm{e}$ and a nuclear part $\hat{H}_\mathrm{N}$,

$$\hat{H} = \hat{H}_\mathrm{e} + \hat{H}_\mathrm{N}, \qquad (2.13)$$

with the nulcear part

$$\hat{H}_\mathrm{N}(\vec{R}) = \hat{T}_\mathrm{N} + \hat{V}_\mathrm{NN}, \qquad (2.14)$$

and the electronic Hamiltonian

$$\hat{H}_\mathrm{e}(\vec{r};\vec{R}) = \hat{T}_\mathrm{e} + \hat{V}_\mathrm{ee} + \hat{V}_\mathrm{eN}, \qquad (2.15)$$

which just depends parametrically on the nuclear configuration (clamped nuclei approximation). Now, a time-independent electronic Schrödinger equation can be defined which is solved separately for a fixed $\vec{R}$,

$$\hat{H}_e \phi_n(\vec{r}; \vec{R}) = E_n(\vec{R}) \phi_n(\vec{r}; \vec{R}). \tag{2.16}$$

Since for every nuclear configuration $\vec{R}$ the electronic wave functions $\{\phi_n\}$ form a complete basis (which is assumed to be discrete), the total wave function $\Phi(\vec{r}, \vec{R})$ can be expanded in this basis (Born-Huang-expansion),

$$\Phi(\vec{r}, \vec{R}) = \sum_n \phi_n(\vec{r}; \vec{R}) \psi_n(\vec{R}), \tag{2.17}$$

where the expansion coefficients $\{\psi_n\}$ depend on the nuclear coordinates. The basis in Eq. (2.17) can now be inserted in Eq. (2.2) and $\langle \phi_m |$ is projected from the left onto the resulting equation,

$$\sum_n \left[(\hat{T}_\mathrm{N} + V_n(\vec{q})) \delta_{mn} - \frac{1}{2} (T^{(2)}_{mn} + 2\vec{T}^{(1)}_{mn} \cdot \vec{\nabla}) \right] \psi_n(\vec{q}) = E \delta_{nm} \psi_m(\vec{q}), \tag{2.18}$$

with the potential

$$V_n(\vec{q}) = E_n(\vec{q}) + \langle \phi_n | \hat{V}_\mathrm{NN}(\vec{q}) | \phi_n \rangle , \tag{2.19}$$

and the nonadiabatic coupling elements

$$\vec{T}^{(1)}_{mn} = \langle \phi_m | \vec{\nabla} | \phi_n \rangle \tag{2.20}$$

$$T^{(2)}_{mn} = \langle \phi_m | \Delta | \phi_n \rangle . \tag{2.21}$$

Eq. (2.18) is formulated in mass-weighted coordinates $\vec{q}$ and the operators in Eq. (2.20) and Eq. (2.21) contain multidimensional derivatives with respect to these coordinates. In the Born-Oppenheimer approximation the nonadiabatic coupling elements are neglected which simplifies Eq. (2.18) to

$$\left(\hat{T}_\mathrm{N} + V_n \right) \psi_n(\vec{q}) = E \psi_n(\vec{q}). \tag{2.22}$$

Now it becomes obvious that ψ_n represents a nuclear wave function. V_n is called the potential energy surface and equals the mean electronic potential in which the nuclei move. Eq. (2.22) makes it possible to evaluate the nuclei's wave function separately for every electronic state n. Therefore, the first task is to solve the electronic eigenvalue problem in Eq. (2.16).

2.2 Electronic structure

In the following section different methods to solve the electronic Schrödinger equation will be presented. At first, the Hartree-Fock (HF) method, as a wave function based ansatz, is going to be discussed. At second, the idea of density functional theory and several functionals, as well as their (dis-)advantages will be introduced and debated. Finally, the section will be concluded by a brief presentation of the principles of periodic bulk calculation. In the whole section the nuclear coordinates $\vec{R}$, on which the electronic wave function depends parametrically, are omitted. If not stated otherwise the textbooks of Jensen,[105] Szabo and Ostlund,[106] Koch and Holthausen[107] as well as of Ashcroft and Mermin[108] were used as references.

2.2.1 Hartree-Fock method

Every fermionic wave function has to obey the Pauli principle, stating that the wave function is antisymmetric with respect to the interchange of two particles. A way to include this prerequisite in the mathematical expression of the N-electron wave function, is by using a determinant,

$$\Psi^{\mathrm{SD}}(\vec{x}_1, ..., \vec{x}_N) = \frac{1}{\sqrt{N!}} \begin{vmatrix} \chi_1(\vec{x}_1) & \cdots & \chi_N(\vec{x}_1) \\ \vdots & \ddots & \vdots \\ \chi_1(\vec{x}_N) & \cdots & \chi_N(\vec{x}_N) \end{vmatrix}. \tag{2.23}$$

These Slater determinants are built up from spin orbitals

$$\chi(\vec{x}) = \phi(\vec{r}) \cdot g(\omega) \tag{2.24}$$

with the spin function

$$g(\omega) = \begin{cases} \alpha(\omega) \\ \beta(\omega) \end{cases} \tag{2.25}$$

and a spatial part ϕ. $\alpha(\omega)$ and $\beta(\omega)$ in Eq. (2.25) describe the two possible orientations of a single electron's spin, and $\vec{x}$ in Eq. (2.24) denotes both spin and space coordinates, ω and $\vec{r}$.

The Hartree-Fock method starts with the assumption that the total wave function can be described by a single Slater determinant, or a single configuration state function for open-shell systems. For the sake of convenience a closed-shell system is assumed in the following. The energy expectation value for a Hartree-Fock wave

function can be written as

$$E_0\left[\{\chi_a\}\right] = \sum_{a=1}^{N}[a|h|a] + \frac{1}{2}\sum_{a=1}^{N}\sum_{b=1}^{N}[aa|bb] - [ab|ba] \tag{2.26}$$

with the one-, and two-electron integrals in chemist's notation

$$[i|h|j] = \int \mathrm{d}\vec{x}\chi_i^*(\vec{x})\hat{h}(\vec{r})\chi_j(\vec{x}) \tag{2.27}$$

$$[ij|kl] = \int \mathrm{d}\vec{x}_1\mathrm{d}\vec{x}_2\chi_i^*(\vec{x}_1)\chi_j(\vec{x}_1)\frac{1}{r_{12}}\chi_k^*(\vec{x}_2)\chi_l(\vec{x}_2), \tag{2.28}$$

and the one-particle operator

$$\hat{h}(i) = -\frac{1}{2}\Delta_i - \sum_{\alpha}\frac{Z_\alpha}{r_{i\alpha}}. \tag{2.29}$$

Interparticle distances are denoted as $|\vec{R}_\alpha - \vec{r}_i| = r_{i\alpha}$ and $|\vec{r}_1 - \vec{r}_2| = r_{12}$, respectively. According to Eq. (2.26) the total energy is a functional of the set of spin orbitals $\{\chi_a\}$. Following the Rayleigh-Ritz variational principle, the best wave function, i.e. the optimal set of spin orbitals, minimizes Eq. (2.26). This set can be obtained by using the method of Lagrange multipliers, with the constraint $\langle a \,|\, b\rangle = \delta_{ab}$, which finally leads to the canonical Hartree-Fock equations,

$$\hat{f}(i)\,|\chi_a\rangle = \left(\hat{h}(i) + \hat{v}^{\mathrm{HF}}(i)\right)|\chi_a\rangle = \varepsilon_a\,|\chi_a\rangle\,, \tag{2.30}$$

where $\hat{f}$ is called Fock operator and ε_a can be associated with a spin orbital energy. Eq. (2.30) is basically a Schrödinger equation of an electron moving in the Hartree-Fock potential $\hat{v}^{\mathrm{HF}}$,

$$\hat{v}^{\mathrm{HF}}(i) = \sum_{b\neq a}\left(\hat{J}_b(i) - \hat{K}_b(i)\right), \tag{2.31}$$

which describes the effective potential experienced by an electron i due to the presence of the remaining $(N-1)$ electrons. The two terms in Eq. (2.31) are called Coulomb and exchange operators. The Coulomb operator

$$\hat{J}_b(1)\chi_a(1) = \left[\int \mathrm{d}\vec{x}_2\chi_b^*(2)\frac{1}{r_{12}}\chi_b(2)\right]\chi_a(1) \tag{2.32}$$

can be interpreted as the interaction of an electron in χ_a with the total averaged potential arising from the $(N-1)$ electrons in the remaining spin orbitals. The

second term, the exchange operator

$$\hat{K}_b(1)\chi_a(1) = \left[\int \mathrm{d}\vec{x}_2 \chi_b^*(2)\frac{1}{r_{12}}\chi_a(2)\right]\chi_b(1), \tag{2.33}$$

describes the possibility of two electrons with parallel spin to interchange. It is a consequence of the Pauli principle and in contrast to the Coulomb operator, the exchange operator is nonlocal since the result of acting with $\hat{K}_b$ on χ_a depends on the value of χ_a throughout all space.
In the Hartree-Fock approach, the original N-particle Schrödinger equation is transformed to the N one-particle Hartree-Fock equations. Solving these one-particle problems is much easier than the general N-electron equation. Since the solutions of Eq. (2.30) are contained in the Fock operator via the Coulomb- and exchange-operators these equations have to be solved iteratively until self-consistency. However, it can be rather difficult to solve these integro-differential equations. Therefore, Roothaan[109] and Hall[110] proposed an expansion of the spatial molecular orbitals $\{\phi_i\}$ into a set of K atomic orbitals $\{\varphi_k\}$,

$$\phi_i = \sum_{k=1}^{K} C_{ki}\varphi_k. \tag{2.34}$$

After integrating the spin coordinate out that MO-LCAO (molecular orbitals as linear combination of atomic orbitals) ansatz leads to the Roothaan-Hall equations,

$$\mathbf{FC} = \mathbf{SC}\varepsilon \tag{2.35}$$

with the Fock matrix, $F_{kk'} = \langle\varphi_k|\,\hat{f}\,|\varphi_{k'}\rangle$ and the overlap matrix, $S_{kk'} = \langle\varphi_k\,|\,\varphi_{k'}\rangle$. The matrix $\mathbf{C}$ contains the coefficients from Eq. (2.34), and the orbital energies appear in the diagonal matrix ε. The MO-LCAO ansatz makes it possible to systematically improve the results by increasing the basis set size K. However, due to the single determinant ansatz the electronic interactions are only treated in an averaged way. Therefore the Hartree-Fock energy is always greater than the exact energy of a given state. The difference between the two is called correlation energy. In more advanced wave-function based methods (CASSCF, coupled cluster, Møller-Plesset perturbation theory) as well as DFT methods, one tries to include correlation effects (see Ref. [105–107, 111] for a more detailed discussion).

2.2.2 Density functional theory

The Hartree-Fock approach belongs to a class of methods which describe a system by its wave function. For an N-particle system this function depends on $4N$ co-

ordinates and thus quickly reaches unmanageable sizes. However, the Hamiltonian only contains one- and two-electron terms, i.e. there are only integrals depending on at most six spatial coordinates in the energy expression. Apparently, the wave function contains more information than necessary to evaluate energies and other observables of interest. Hence, it should be possible to obtain these properties by using a function depending on a smaller set of coordinates. And indeed, in the early days of quantum mechanics it was shown by Thomas[112] and Fermi[113] that the energy of a uniform electron gas can be expressed as a functional of the density

$$\rho(\vec{r}) = N \int \cdots \int \mathrm{d}\vec{\omega}_1 \mathrm{d}\vec{x}_2 ... \mathrm{d}\vec{x}_N |\Psi(\vec{x}_1, ..., \vec{x}_N)|^2. \tag{2.36}$$

In 1964 Hohenberg and Kohn introduced and proved two theorems stating that the density can be used to calculate quantum mechanical properties of general systems.[114] Their first theorem states that the energy E_0 of a non-degenerate ground state is a unique functional of the ground state density ρ_0,

$$E_0 = E_0[\rho_0]. \tag{2.37}$$

As a consequence, all terms contributing to the ground state energy can be written as functionals of the ground state density,

$$E_0[\rho_0] = \bar{T}[\rho_0] + \bar{V}_{eN}[\rho_0] + \bar{V}_{ee}[\rho_0], \tag{2.38}$$

where $\bar{T}[\rho_0]$ denotes the average kinetic energy, $\bar{V}_{eN}[\rho_0]$ the average electron-nuclei interaction and $\bar{V}_{ee}[\rho_0]$ the average electron-electron interaction. The second Hohenberg-Kohn theorem states that the variational theorem can be applied to the density, i.e. for every trial density $\tilde{\rho}$ (which obeys $\int \mathrm{d}\vec{r}\tilde{\rho}(\vec{r}) = N$ and $\tilde{\rho} \geq 0, \forall \vec{r}$) it holds that

$$E[\tilde{\rho}] \geq E_0. \tag{2.39}$$

These theorems show that it is possible to reformulate the procedure to obtain ground state energies by using densities instead of wave functions. However, they do not explain how that density can be obtained in practice. In orbital-free DFT, it is the density which is variationally optimized. But the often insufficient description of the kinetic energy causes large errors in the total energy. Therefore, the usual method to evaluate ground state densities and the corresponding energies is based on an idea proposed by Kohn and Sham.[115] They start with a hypothetical system

of non-interacting particles with a total Hamiltonian

$$\hat{H}^{\mathrm{KS}} = \sum_{i=1}^{N} \hat{h}_i^{\mathrm{KS}} = \sum_{i=1}^{N} \left(-\frac{1}{2}\Delta_i + v_S(\vec{r}) \right), \tag{2.40}$$

where $v_S(\vec{r})$ denotes a one-electron potential. An eigenfunction of Eq. (2.40) is a Slater determinant whose spatial orbitals are solutions of the Kohn-Sham equations,

$$\hat{h}_i^{\mathrm{KS}} \phi_i^{\mathrm{KS}} = \varepsilon_i^{\mathrm{KS}} \phi_i^{\mathrm{KS}}. \tag{2.41}$$

The system's density ρ_S can be reconstructed from the Kohn-Sham orbitals $\{\phi_i^{\mathrm{KS}}\}$,

$$\rho_S = \sum_{i=1}^{N} |\phi_i^{\mathrm{KS}}|^2. \tag{2.42}$$

Now, the potential v_S should be chosen such that the density ρ_S of the non-interacting systems equals the exact ground state density ρ_0. In order to see which terms contribute to the potential v_S it is best to start from the expression of the first Hohenberg-Kohn theorem in Eq. (2.38). There, the first term, the average kinetic energy, can be decomposed in a part

$$\bar{T}_S[\rho] = -\frac{1}{2} \sum_{i}^{N} \left\langle \phi_i^{\mathrm{KS}} \middle| \Delta \middle| \phi_i^{\mathrm{KS}} \right\rangle, \tag{2.43}$$

which describes the average kinetic energy of a non-interacting system and a correction term $\Delta\bar{T}$ accounting for correlation effects on the average kinetic energy. The second term in Eq. (2.38) can easily be rewritten as a functional of the density,

$$\bar{V}_{eN}[\rho] = -\sum_{\alpha} Z_\alpha \int \mathrm{d}\vec{r}_1 \frac{\rho(\vec{r}_1)}{r_{1\alpha}}. \tag{2.44}$$

The last energy contribution comes from the electron-electron interaction and is decomposed to

$$\bar{V}_{ee}[\rho] = \frac{1}{2} \int\int \mathrm{d}\vec{r}_1 \mathrm{d}\vec{r}_2 \frac{\rho(\vec{r}_1)\rho(\vec{r}_2)}{r_{12}} + \Delta\bar{V}_{ee}[\rho], \tag{2.45}$$

where the first term (Hartree term) describes the Coulomb repulsion and the second accounts for exchange and correlation parts. Hence, the total energy in Eq. (2.38)

can be rewritten as

$$E_0 = -\frac{1}{2}\sum_i^N \langle \phi_i^{\mathrm{KS}} \,|\, \Delta \,|\, \phi_i^{\mathrm{KS}} \rangle - \sum_\alpha Z_\alpha \int \mathrm{d}\vec{r}_1 \frac{\rho(\vec{r}_1)}{r_{1\alpha}} + \frac{1}{2}\int\int \mathrm{d}\vec{r}_1 \mathrm{d}\vec{r}_2 \frac{\rho(\vec{r}_1)\rho(\vec{r}_2)}{r_{12}} + E_{XC}[\rho]. \tag{2.46}$$

Here, the kinetic and potential correction terms are summed up to the exchange-correlation functional,

$$E_{XC}[\rho] = \Delta\bar{T}[\rho] + \Delta\bar{V}_{ee}[\rho]. \tag{2.47}$$

Now, similar to the Hartree-Fock method the energy in Eq. (2.46) is minimized, but with respect to the Kohn-Sham orbitals, leading to a new formulation of the Kohn-Sham equations

$$\left[-\frac{1}{2}\Delta_1 - \sum_\alpha \frac{Z_\alpha}{r_{1\alpha}} + \int \mathrm{d}\vec{r}_2 \frac{\rho(\vec{r}_2)}{r_{12}} + v_{XC}(\vec{r}_1)\right] \phi_i^{\mathrm{KS}}(\vec{r}_1) = \varepsilon_i^{\mathrm{KS}} \phi_i^{\mathrm{KS}}(\vec{r}_1), \tag{2.48}$$

with the exchange-correlation potential

$$v_{XC}(\vec{r}) = \frac{\delta E_{XC}[\rho(\vec{r})]}{\delta\rho(\vec{r})}. \tag{2.49}$$

Thus the original task of finding v_S was reduced to find an expression for the exchange-correlation potential v_{XC} which would yield the exact ground state density and energy. However, since for most systems the exact exchange-correlation potential v_{XC} is not known the main difficulty in DFT is to find an appropriate approximation to v_{XC}.

One of the simplest expressions for the exchange-correlational functional is based on the local-density approximation (LDA). In that approach, the density is treated locally as a uniform electron gas. In that case the exchange-correlation functional can be written exactly as

$$E_{\mathrm{XC}}[\rho] = \int \mathrm{d}\vec{r}\rho(\vec{r})\varepsilon_{\mathrm{XC}}[\rho], \tag{2.50}$$

where $\varepsilon_{\mathrm{XC}}$ is the exchange-correlation energy per electron in a homogeneous electron gas with density ρ. The exchange-correlation energy can be decomposed in an exchange part ε_{X} and a correlation part ε_{C},

$$\varepsilon_{\mathrm{XC}}[\rho] = \varepsilon_{\mathrm{X}}[\rho] + \varepsilon_{\mathrm{C}}[\rho]. \tag{2.51}$$

For the exchange part there is an analytic expression given by

$$\varepsilon_{\mathrm{X}}[\rho] = -\frac{3}{4}\left(\frac{3\rho}{\pi}\right)^{\frac{1}{3}}. \tag{2.52}$$

For the correlation part there are analytic expressions in the low and high density limit.[116,117] Furthermore, Vosko, Wilk and Nusair developed an analytical fit $\varepsilon_{\mathrm{C}}^{\mathrm{VWN}}$ to cover the whole density range.[118] The LDA exactly describes a unifrom electron gas. For systems with slowly varying density, e.g. metallic systems, that approach can yield reasonable results. However, for most molecular systems LDA produces very inaccurate results due to the inhomogeneous density distributions in molecules.

The inhomogeneous density distribution can be taken into account by expressing the exchange-correlation energy as a functional of the density as well as of the gradient of the density,

$$E_{\mathrm{XC}}[\rho, \vec{\nabla}\rho] = \int \mathrm{d}\vec{r} f(\rho(\vec{r}), \vec{\nabla}\rho(\vec{r})). \tag{2.53}$$

There are different flavours of this generalized gradient approximation (GGA), many of them contain empirical parameters. A very popular functional, based on analytical parameters, was developed by Perdew, Burke and Enzerhof (PBE[119]). They start with the LDA expressions and rescale the exchange part with a function $F(x)$,

$$\varepsilon_{\mathrm{X}}^{\mathrm{PBE}} = \varepsilon_{\mathrm{X}}^{\mathrm{LDA}} F(x) \tag{2.54}$$

and shift the correlation part by a function $H(t)$,

$$\varepsilon_{\mathrm{C}}^{\mathrm{PBE}} = \varepsilon_{\mathrm{C}}^{\mathrm{LDA}} + H(t). \tag{2.55}$$

The functions $F(x)$ and $H(t)$ depend on non-empirical parameters, which are derived by demanding the functional to obey some fundamental properties of DFT functionals (see Ref. [105] for more information).
Due to the approximation of the Hamilton operator in DFT, the functionals generally do not capture effects which naturally arise in (accurate) wave-function based methods, e.g. cancellation of self-interaction and long-range electron correlation (dispersion).
In order to partly correct for the self-interaction error hybrid functionals were developed which use some amount of Hartree-Fock exchange energy to correct for the insufficient description of exchange in many DFT functionals. There are many different hybrid approaches which differ in the amount of exact exchange and the underlying functional,[120–123] e.g. the PBE0 hybrid functional is based on the PBE

functional and mixes DFT and Hartree-Fock exchange in a 3:1 ratio,[124,125]

$$E_{\mathrm{XC}}^{\mathrm{PBE0}} = E_{\mathrm{C}}^{\mathrm{PBE}} + \frac{1}{4}E_{\mathrm{X}}^{\mathrm{HF}} + \frac{3}{4}E_{\mathrm{X}}^{\mathrm{PBE}}. \tag{2.56}$$

The inclusion of dispersive effects in DFT is usually performed semiempirically with an ansatz suggested by Grimme,[126] who corrects the DFT energy of a certain functional with a dispersive term,

$$E_{\mathrm{DFT-D3}} = E_{\mathrm{DFT}} + E_{\mathrm{disp}}, \tag{2.57}$$

with $E_{\mathrm{disp}} = E^{(2)} + E^{(3)}$. The two-body contribution is given by

$$E^{(2)} = -\sum_{AB}\sum_{n=6,8,\ldots}\frac{C_n^{AB}}{r_{AB}^n} f_{d,n}(r_{AB}), \tag{2.58}$$

where the first sum runs over all atom pairs AB with a nuclear distance of r_{AB}. C_n^{AB} is the averaged nth-order dispersion coefficient of the pair AB and $f_{d,n}(r_{AB})$ is a damping function defining the range of the dispersion correction. The three-body term is calculated by

$$E^{(3)} = \sum_{ABC} f_{d,(3)}(\bar{r}_{ABC}) E^{ABC} \tag{2.59}$$

with the geometrically averaged radii $\bar{r}_{ABC}$ and the dispersion term E^{ABC} derived from third-order perturbation theory.

2.2.3 Periodic bulk calculations

The description of periodic structures is typically done by means of a Bravais lattice, which is defined as a set of all points $\vec{R}$ in position space given by

$$\vec{R} = n_1\vec{a}_1 + n_2\vec{a}_2 + n_3\vec{a}_3, \quad n_1, n_2, n_3 \in \mathbb{Z}. \tag{2.60}$$

The lattice is spanned by the primitive vectors $\vec{a}_1, \vec{a}_2, \vec{a}_3$, whose choice is not unique for a given Bravais lattice. In order to describe periodic systems it is only necessary to consider the lattice's unit cell, defined as the smallest possible volume in position space which can be used to build up the whole lattice by translating this cell along $\vec{R}$. If the unit cells contains only one atom it is called primitive. It is possible that the chosen primitive cell does not represent the whole symmetry of the system. However, it is always possible to find a unit cell with the whole symmetry (Wigner-Seitz cell).

Usually, the theoretical description of periodic systems is not performed in position

(real) but in momentum (reciprocal) space. For a given Bravais lattice $\{\vec{R}\}$ it is possible to find a reciprocal space $\{\vec{K}\}$ whose points also form a Bravais lattice and are given by

$$\vec{K} = h\vec{b}_1 + k\vec{b}_2 + l\vec{b}_3 \quad h,k,l \in \mathbb{Z}, \tag{2.61}$$

where h,k,l are called Miller indices. Since the real and reciprocal space are connected by $e^{\vec{K}\vec{R}} = 1$, the primitive basis in reciprocal space is written as

$$\vec{b}_1 = 2\pi \frac{\vec{a}_2 \times \vec{a}_3}{\vec{a}_1 (\vec{a}_2 \times \vec{a}_3)}, \tag{2.62}$$

$$\vec{b}_2 = 2\pi \frac{\vec{a}_3 \times \vec{a}_1}{\vec{a}_1 (\vec{a}_2 \times \vec{a}_3)}, \tag{2.63}$$

$$\vec{b}_3 = 2\pi \frac{\vec{a}_1 \times \vec{a}_2}{\vec{a}_1 (\vec{a}_2 \times \vec{a}_3)}. \tag{2.64}$$

$$\tag{2.65}$$

The Wigner-Seitz cell in this reciprocal lattice is called first Brillouin zone.
The quantum mechanical description of periodic systems is usually done in a one-electron picture as in Eq. (2.30) or Eq. (2.40). If the effective potential obeys the system's translational symmetry, i.e. $V(\vec{r}) = V(\vec{r}+\vec{R})$, the Bloch theorem[127] states that every single-particle wave function can be written as

$$\phi_{n\vec{k}}(\vec{r}) = e^{i\vec{k}\vec{r}} u_{n\vec{k}}(\vec{r}) \tag{2.66}$$

with the amplitude function $u_{n\vec{k}}(\vec{r})$ satisfying the periodicity of the lattice, i.e.

$$u_{n\vec{k}}(\vec{r}) = u_{n\vec{k}}(\vec{r}+\vec{R}). \tag{2.67}$$

The index n is called band and describes the fact that for every $\vec{k}$ there are several independent eigenstates. Since in practical calculations it is not possible to consider an infinite crystal but only a finite number of unit cells one has to impose Born-von-Kármán boundary conditions

$$\Psi(\vec{r}) = \Psi(\vec{r} + N_i\vec{a}_i), \quad i = 1,2,3 \tag{2.68}$$

with the integers N_i linked to the total number of primitive cells N by $N = N_1N_2N_3$.

2.3 Open Quantum Systems

The following sections begin with a brief introduction of the concept of density operators and reduced density operators. Based on that concept, a quantum master equation of the reduced density operator will be derived for a system weakly coupled to an environment. Afterwards, the principle of a piecewise deterministic process will be explained and the equivalence between the quantum master equation and the PDP will be shown. In the last part, the coupling of molecular vibrations to surface electrons in the classical as well as the quantum mechanical regime will be explained by means of the concept of electronic friction. If not stated otherwise the textbooks of Breuer and Petruccione,[128] Tannor,[101] Nolting,[102] Zwanzig[129] and Joswig and Springborg[130] were used as references.

2.3.1 Density operators

Until now we only considered quantum systems in pure states, i.e. states which can be described by a vector $|\Psi\rangle$ in Hilbert space. However, for most macroscopic, and even some microscopic, systems the exact state is often not known. Therefore, the system is described in a statistical fashion by means of the density operator,

$$\rho(t) = \sum_m p_m \left|\Psi_m(t)\right\rangle \left\langle\Psi_m(t)\right|, \tag{2.69}$$

where p_m is the probability to find the system in a pure state $|\Psi_m(t)\rangle$. By expanding the pure states in a time-independent basis $\{\psi_i\}$ the incoherent superposition of states in Eq. (2.69) can be reformulated as

$$\rho(t) = \sum_{ij} P_{ij}(t) \left|\psi_i\right\rangle \left\langle\psi_j\right|, \tag{2.70}$$

where $P_{ij}(t)$ denotes the density matrix. The diagonal elements of that matrix are the populations of the basis $\{\psi_i\}$ and the non-diagonal elements describe the coherences between these states. Taking the time-derivative of Eq. (2.69) and using Eq. (2.1) leads to the Liouville-von-Neumann equation

$$\frac{\mathrm{d}}{\mathrm{d}t}\rho(t) = -i\left[\hat{H}(t), \rho(t)\right], \tag{2.71}$$

which characterizes the dynamical behaviour of the density operator. Any expectation value of an operator $\hat{A}$ can be calculated by

$$\left\langle \hat{A} \right\rangle = \mathrm{tr}(\hat{A}\rho), \tag{2.72}$$

where tr() denotes the trace over all basis functions of ρ. When describing complex systems it is often useful to decompose the complete system in subsystems. For example, in the case of two subsystems the complete Hilbert space $\mathcal{H}$ can be expressed as a tensor product of the two subspaces, $\mathcal{H} = \mathcal{H}_1 \otimes \mathcal{H}_2$. The expectation value of an operator $\hat{A}^{(1)}$ only acting on subspace $\mathcal{H}_1$ is then given by

$$\left\langle \hat{A}^{(1)} \right\rangle = \mathrm{tr}_1(\hat{A}^{(1)}\rho_1), \tag{2.73}$$

where the trace is performed over the basis of subspace $\mathcal{H}_1$. The density operator in Eq. (2.73) is called reduced density operator and it is extracted from the complete density operator ρ by tracing over all basis functions of subsystem $\mathcal{H}_2$,

$$\rho_1 = \mathrm{tr}_2(\rho). \tag{2.74}$$

In general, the reduced density operator describes a mixed ensemble even if the complete system is in a pure state.

2.3.2 Quantum master equation in the weak coupling limit

A system S which can exchange energy and particles with an environment (or bath) B is called an open system. In general, the composite system $S + B$ is assumed to be closed. The Hamiltonian for such a system is given by

$$\hat{H}(t) = \hat{H}_\mathrm{S} \otimes \mathbb{I}_\mathrm{B} + \mathbb{I}_\mathrm{S} \otimes \hat{H}_\mathrm{B} + \hat{H}_\mathrm{I}(t), \tag{2.75}$$

where $\hat{H}_\mathrm{S}$ ($\hat{H}_\mathrm{B}$) is the system (bath) Hamiltonian and $\hat{H}_\mathrm{I}(t)$ describes the generally time-dependent interaction between system and bath. The identity matrix in the Hilbert space of the system (bath) is denoted by $\mathbb{I}_\mathrm{S}$ ($\mathbb{I}_\mathrm{B}$). In the interaction picture, the Liouville-von Neumann equation for the complete system is simply

$$\frac{\mathrm{d}}{\mathrm{d}t}\rho_\mathrm{SB}(t) = -i\left[\hat{H}_\mathrm{I}(t), \rho_\mathrm{SB}(t)\right], \tag{2.76}$$

which has the formal solution

$$\rho_\mathrm{SB}(t) = \rho_\mathrm{SB}(0) - i\int_0^t \mathrm{d}s \left[\hat{H}_\mathrm{I}(s), \rho_\mathrm{SB}(s)\right]. \tag{2.77}$$

However, for many phenomena the description of the complete system $S + B$ is much too complicated because the bath may have (infinitely) many degrees of freedom leading to a hierarchy of (infinitely) many coupled equations of motion. Besides, often the bath modes are not known exactly nor can they be controlled experimentally. And even if the complete solution ρ_SB can be found, the relevant information

about the open system S has to be extracted from that solution.
Therefore, one tries to formulate an equation of motion for the open system S only by inserting Eq. (2.77) in Eq. (2.76) and tracing over the bath modes. After that, an equation of motion for the open system S is obtained,

$$\frac{\mathrm{d}}{\mathrm{d}t}\rho_{\mathrm{S}}(t) = -i\ \mathrm{tr}_{\mathrm{B}}\left[\hat{H}_{\mathrm{I}}(t), \rho_{\mathrm{SB}}(0)\right] - \int_0^t \mathrm{d}s\ \mathrm{tr}_{\mathrm{B}}\left[\hat{H}_{\mathrm{I}}(t), \left[\hat{H}_{\mathrm{I}}(s), \rho_{\mathrm{SB}}(s)\right]\right], \tag{2.78}$$

with the density matrix of the open system given by

$$\rho_{\mathrm{S}}(t) = \mathrm{tr}_{\mathrm{B}}\{\rho_{\mathrm{SB}}(t)\}. \tag{2.79}$$

The first term in Eq. (2.78) is neglected since it is assumed that in the initial density no interaction is present. However, the aim is to have an equation of motion depending on ρ_{S}. But in Eq. (2.78) the density ρ_{SB} still appears. To eliminate it from the expression in Eq. (2.78) the total density is replaced by a tensor product,

$$\rho_{\mathrm{SB}}(t) \approx \rho_{\mathrm{S}}(t) \otimes \rho_{\mathrm{B}}. \tag{2.80}$$

This approximation is known as the Born approximation. It replaces the total density by a tensor product of the subsystems because they are assumed to interact only weakly. Due to the weak coupling there is no induced change of the bath's density on the time scale of the system's evolution. Therefore, the bath stays in its initial state, which is chosen to be the thermal equilibrium. The resulting equation of motion,

$$\frac{\mathrm{d}}{\mathrm{d}t}\rho_{\mathrm{S}}(t) = -\int_0^t \mathrm{d}s\ \mathrm{tr}_{\mathrm{B}}\left[\hat{H}_{\mathrm{I}}(t), \left[\hat{H}_{\mathrm{I}}(s), \rho_{\mathrm{S}}(s) \otimes \rho_{\mathrm{B}}\right]\right], \tag{2.81}$$

can be modified further by employing the Markov approximation. At first, it is assumed that the change of the density at time t only depends on the density at that time which leads to the Redfield equation,

$$\frac{\mathrm{d}}{\mathrm{d}t}\rho_{\mathrm{S}}(t) = -\int_0^t \mathrm{d}s\ \mathrm{tr}_{\mathrm{B}}\left[\hat{H}_{\mathrm{I}}(t), \left[\hat{H}_{\mathrm{I}}(s), \rho_{\mathrm{S}}(t) \otimes \rho_{\mathrm{B}}\right]\right]. \tag{2.82}$$

However, this equation is local in time but it is not Markovian since its time evolution still depends on the preparation at $t = 0$. Thus, the system's dynamics is not described by a dynamical semigroup[1], i.e. the diagonal elements of the density matrix could be negative. Two further steps are necessary to get an equation of

[1]The transformation of a reduced density matrix at time $t = 0$ to a fixed time $t > 0$ can be formulated as $\rho_{\mathrm{S}}(t) = V(t)\rho_{\mathrm{S}}(0) = \mathrm{tr}_{\mathrm{B}}\{U(t,0)\,[\rho_{\mathrm{S}}(0) \otimes \rho_{\mathrm{B}}]\,U^{\dagger}(t,0)\}$, with the time-evolution operator U. For fixed time t and bath density ρ_{B} the operator $V(t)$ defines a dynamical map. If t is varied the one-parameter family $\{V(t)|t \geq 0\}$ of maps forms a dynamical semigroup.

motion fulfilling the properties of such a semigroup. At first, the integration variable s is substituted by $t - s$ and the upper integration limit is extended to infinity,

$$\frac{\mathrm{d}}{\mathrm{d}t}\rho_{\mathrm{S}}(t) = -\int_0^\infty \mathrm{d}s \ \mathrm{tr}_{\mathrm{B}}\left[\hat{H}_{\mathrm{I}}(t), \left[\hat{H}_{\mathrm{I}}(t-s), \rho_{\mathrm{S}}(t)\otimes\rho_{\mathrm{B}}\right]\right]. \tag{2.83}$$

This is possible if the integrand decays sufficiently fast for $s \gg \tau_{\mathrm{B}}$, where τ_{B} is the time scale over which the bath correlation function decays. This implies that $\tau_{\mathrm{R}} \gg \tau_{\mathrm{B}}$ with the time scale τ_{R} over which the system changes significantly. All approximations employed so far are known as Born-Markov approximation. The second approximative step is the rotating wave approximation which finally guarantees a probabilistic interpretation of ρ_{S}. It starts with a spectral decomposition of the interaction term in the Schrödinger picture into

$$\hat{H}_{\mathrm{I}} = \sum_\alpha \hat{A}_\alpha(t)\otimes\hat{B}_\alpha(t), \tag{2.84}$$

where $\hat{A}_\alpha$ and $\hat{B}_\alpha$ are the unitary system and bath operators, respectively. The system operators can be expanded in a complete basis $\{\hat{A}_\alpha(\omega)\}$ with

$$\hat{A}_\alpha(\omega) = \sum_{\varepsilon'-\varepsilon=\omega} \Pi(\varepsilon)\hat{A}_\alpha\Pi(\varepsilon'), \tag{2.85}$$

where $\Pi(\varepsilon)$ is a projection operator onto an eigenspace of the system S with eigenenergy ε. The spectrum of $\hat{H}_{\mathrm{S}}$ is supposed to be discrete. It follows from Eq. (2.85) that the system operators can be expressed in the interaction picture as

$$e^{i\hat{H}_{\mathrm{S}}t}\hat{A}_\alpha(\omega)e^{-\hat{H}_{\mathrm{S}}t} = e^{-i\omega t}\hat{A}_\alpha(\omega). \tag{2.86}$$

Now, with Eq. (2.84) and Eq. (2.86) the interaction term can be written in the interaction picture,

$$\hat{H}_{\mathrm{I}}(t) = \sum_{\omega,\alpha} e^{-i\omega t}\hat{A}_\alpha(\omega)\otimes\hat{B}_\alpha(t), \tag{2.87}$$

with the bath operator

$$\hat{B}_\alpha(t) = e^{i\hat{H}_{\mathrm{B}}t}\hat{B}_\alpha e^{-i\hat{H}_{\mathrm{B}}t}. \tag{2.88}$$

Next, Eq. (2.87) can be inserted into Eq. (2.83) leading to,

$$\frac{\mathrm{d}}{\mathrm{d}t}\rho_{\mathrm{S}}(t) = \int_0^\infty \mathrm{d}s\ \mathrm{tr}_{\mathrm{B}}\{\hat{H}_{\mathrm{I}}(t-s)\rho_{\mathrm{S}}(t)\rho_{\mathrm{B}}\hat{H}_{\mathrm{I}}(t) - \hat{H}_{\mathrm{I}}(t)\hat{H}_{\mathrm{I}}(t-s)\rho_{\mathrm{S}}(t)\rho_{\mathrm{B}}\} + \mathrm{h.c.} \tag{2.89}$$

$$= \sum_{\omega,\omega'}\sum_{\alpha,\beta} e^{i(\omega'-\omega)t}\Gamma_{\alpha\beta}(\omega)\left[\hat{A}_\beta(\omega)\rho_{\mathrm{S}}(t)\hat{A}_\alpha^\dagger(\omega') - \hat{A}_\alpha^\dagger(\omega')\hat{A}_\beta(\omega)\rho_{\mathrm{S}}(t)\right] + \mathrm{h.c.}, \tag{2.90}$$

with the hermitean conjugate h.c. and the one-sided Fourier transform

$$\Gamma_{\alpha\beta}(\omega) = \int_0^\infty \mathrm{d}s\ e^{i\omega s}\langle\hat{B}_\alpha^\dagger(t)\hat{B}_\beta(t-s)\rangle \tag{2.91}$$

$$= \int_0^\infty \mathrm{d}s\ e^{i\omega s}\langle\hat{B}_\alpha^\dagger(s)\hat{B}_\beta(0)\rangle. \tag{2.92}$$

Since ρ_{B} is stationary the correlation function in Eq. (2.92) is homogeneous in time and hence the correlation tensor $\Gamma_{\alpha\beta}$ is time-independent. It can decomposed in a real and an imaginary part,

$$\Gamma_{\alpha\beta}(\omega) = \frac{1}{2}\gamma_{\alpha\beta}(\omega) + iS_{\alpha\beta}(\omega). \tag{2.93}$$

Usually, the time scale of the system's relaxation τ_{R} is considered to be large compared to the time scale of the system's intrinsic dynamics $\tau_{\mathrm{S}} \sim |\omega - \omega'|^{-1}$, i.e. $\tau_{\mathrm{R}} \gg \tau_{\mathrm{S}}$. In that case, all terms with $\omega \neq \omega'$ in Eq. (2.90) can be neglected since they oscillate very fast on the time scale τ_{R} and hence average out. This rotating wave approximation leads to the final equation of motion,

$$\frac{\mathrm{d}}{\mathrm{d}t}\rho_{\mathrm{S}}(t) = \sum_{\omega}\sum_{\alpha,\beta}\Gamma_{\alpha\beta}(\omega)\left[\hat{A}_\beta(\omega)\rho_{\mathrm{S}}(t)\hat{A}_\alpha^\dagger(\omega) - \hat{A}_\alpha^\dagger(\omega)\hat{A}_\beta(\omega)\rho_{\mathrm{S}}(t)\right] + \mathrm{h.c.} \tag{2.94}$$

$$= -i\left[\hat{H}_{\mathrm{LS}}, \rho_{\mathrm{S}}(t)\right] + \mathcal{D}(\rho_{\mathrm{S}}(t)). \tag{2.95}$$

Eq. (2.95) is a dissipative Liouville-von Neumann equation in the interaction picture with the Lamb shift Hamiltonian

$$\hat{H}_{\mathrm{LS}} = \sum_{\omega}\sum_{\alpha\beta} S_{\alpha\beta}(\omega)\hat{A}_\alpha^\dagger(\omega)\hat{A}_\beta(\omega), \tag{2.96}$$

which leads to a renormalization of the system's unperturbed eigenstates, and a dissipator

$$\mathcal{D}(\rho_S) = \sum_{\omega} \sum_{\alpha\beta} \gamma_{\alpha\beta}(\omega) \left[A_\beta(\omega) \rho_S A_\alpha^\dagger(\omega) - \frac{1}{2} \{ A_\alpha^\dagger(\omega) A_\beta(\omega), \rho_S \} \right]. \tag{2.97}$$

The last term in Eq. (2.97) is an anticommutator. By diagonalizing $\gamma_{\alpha\beta}$ in Eq. (2.97) the expression can be brought into Lindblad form. Additionally, when transforming Eq. (2.95) back to the Schrödinger picture the dissipative Liouville-von-Neumann equation takes the form

$$\frac{\mathrm{d}}{\mathrm{d}t} \rho_S(t) = -i \left[\hat{H}_S, \rho_S(t) \right] + \sum_{\alpha} \gamma_\alpha \left[\hat{A}_\alpha \rho_S(t) \hat{A}_\alpha^\dagger - \frac{1}{2} \{ \hat{A}_\alpha^\dagger \hat{A}_\alpha, \rho_S(t) \} \right], \tag{2.98}$$

where, in the spirit of weak coupling, the Lamb-shift Hamiltonian was neglected.

2.3.3 Piecewise Deterministic Processes

A system's state $x(t)$ that follows a deterministic time evolution can be described by a differential equation of the form

$$\frac{\mathrm{d}}{\mathrm{d}t} x(t) = g(x(t)) \tag{2.99}$$

where g is a D-dimensional vector field, which in the following is assumed to be not explicitely time-dependent. When dealing with stochastic processes, the system's evolution is typically described by means of the propagator $T(x, t|x', t')$ which is defined as the probability to find the system in state x at time t under the condition that it was in state x' at time t'. As a special case of a stochastic process, also the deterministic time evolution can be reformulated with a propagator. For a short time interval $\Delta t = t - t'$ it is simply given by

$$T(x, t|x', t') = \delta(x - x' - g(x')\Delta t) + \mathcal{O}(\Delta t^2), \tag{2.100}$$

where the flow of Eq. (2.99) is expanded to first order. The propagator in Eq. (2.100) can be used to construct the propagator of a piecewise deterministic process (PDP). The latter is defined as a stochastic process in which a system follows a deterministic time evolution subjected to instantaneous jumps. In order to account for the jump process the expression of Eq. (2.100) has to be modified,

$$T(x, t + \Delta t|x', t) = (1 - \Gamma(x')\Delta t)\delta(x - x' - g(x')\Delta t) + W(x|x')\Delta t + \mathcal{O}(\Delta t^2), \tag{2.101}$$

where $W(x|x')$ is the jump rate from x' to x and $\Gamma(x') = \int \mathrm{d}x W(x|x')$ describe the total jump rate out of state x'. Thus, the first term in Eq. (2.101) is the probability that no jump occurs in Δt, whereas the second term is the probability that a jump from x' to x occurs in Δt. Differentiation of Eq. (2.101) leads to the Liouville master equation,

$$\frac{\partial}{\partial t}T(x,t|x',t') = -\sum_i \frac{\partial}{\partial x_i}\left[g_i(x)T(x,t|x',t')\right] + \int \mathrm{d}x''\left[W(x|x'')T(x'',t|x',t') - W(x''|x)T(x,t|x',t')\right], \quad (2.102)$$

where the sum describes the deterministic drift and the integral is a balance term of jumps in and from state x. From Eq. (2.102) an expression for the evolution of the probability density $P(x,t)$ can be derived,

$$\frac{\partial}{\partial t}P(x,t) = -\sum_i \frac{\partial}{\partial x_i}\left[g_i(x)P(x,t)\right] + \int \mathrm{d}x''\left[W(x|x'')P(x'',t) - W(x''|x)P(x,t)\right], \quad (2.103)$$

where the probability density and the propagator are connected via

$$P(x,t) = \int \mathrm{d}x' T(x,t|x',t_0)P(x',t_0). \quad (2.104)$$

If the PDP is described in Hilbert space Eq. (2.103) takes the following form,

$$\frac{\partial}{\partial t}P[\Psi,t] = -i\int \mathrm{d}x\left\{\frac{\delta}{\delta\Psi(x)}G(\Psi)(x) - \frac{\delta}{\delta\Psi^*(x)}G(\Psi)^*(x)\right\}P[\Psi,t] + \int D\tilde{\Psi}D\tilde{\Psi}^*\left\{W[\Psi|\tilde{\Psi}]P[\tilde{\Psi},t] - W[\tilde{\Psi}|\Psi]P[\Psi,t]\right\}, \quad (2.105)$$

with a non-linear operator G. Here, $D\Psi$ describes a functional volume element in Hilbert space. After having introduced the concept of a piecewise deterministic process it can be shown that such processes can be employed to unravel the quantum master Eq. (2.98). Unravelling the master equation means that instead of propagating the density matrix (covariance matrix)

$$\rho_S(x,x',t) = E[\Psi(x,t)\Psi^*(x',t)] = \int D\Psi D\Psi^* P[\Psi,t]\Psi(x)\Psi^*(x'), \quad (2.106)$$

with the help of the dissipative Liouville-von Neumann Eq. (2.98), it is possible to propagate the probability density $P[\Psi,t]$ via Eq. (2.105) and reconstruct the covariance matrix from the realizations of the stochastic process (see Fig. (2.1)). The equivalence between these two approaches can be shown by taking the derivative of

$$\begin{array}{ccc} \rho_{\mathrm{S}}(t_0) & \xrightarrow{V(t,t_0)} & \rho_{\mathrm{S}}(t) \\ {\scriptstyle E[|\Psi_0\rangle\langle\Psi_0|]}\uparrow & & \uparrow{\scriptstyle E[|\Psi(t)\rangle\langle\Psi(t)|]} \\ P[\Psi_0,t_0] & \xrightarrow{T[\Psi,t|\Psi_0,t_0]} & P[\Psi,t] \end{array}$$

Figure 2.1: The density matrix ρ_{S} can be propagated a) directly with the help of a superoperator $V(t,t_0)$ mapping the density from time t_0 to t, or b) indirectly by propagating the probability density $P[\Psi,t]$ of a stochastic process and reconstructing the density afterwards by means of the covariance matrix $E[|\Psi\rangle\langle\Psi|]$. The figure is reproduced from Ref. [128]

Eq. (2.106) which leads to

$$\frac{\partial}{\partial t}\rho_{\mathrm{S}}(x,x',t) = \int D\Psi D\Psi^* \frac{\partial}{\partial t} P[\Psi,t]\Psi(x)\Psi^*(x') = \frac{\partial}{\partial t}\rho_{\mathrm{S}}\Big|_{\mathrm{L}} + \frac{\partial}{\partial t}\rho_{\mathrm{S}}\Big|_{\mathrm{J}}, \tag{2.107}$$

consisting of a rate of change of the density induced by the Liouvillian part (index L) and a rate induced by the jump part in Eq. (2.105) (index J). According to Eq. (2.105) the Liouvillian part becomes

$$\begin{aligned} \frac{\partial}{\partial t}\rho_{\mathrm{S}}\Big|_{\mathrm{L}} &= i\int D\Psi D\Psi^* \int \mathrm{d}y \Psi(x)\Psi^*(x')\left\{\frac{\delta}{\delta\Psi(y)}G\left(\Psi\right)(y) - \frac{\delta}{\delta\Psi^*(y)}G(\Psi)^*(y)\right\}P[\Psi,t] \\ &= -i\int D\Psi D\Psi^*\left\{G(\Psi)(x)\Psi^*(x') - \Psi(x)G^*(\Psi)(x')\right\}P[\Psi,t] \\ &= -i\left(\hat{H}\rho_{\mathrm{S}} - \rho_{\mathrm{S}}\hat{H}^\dagger\right) + \sum_i \gamma_i E\left[||\hat{A}_i\Psi||^2\Psi(x)\Psi^*(x')\right], \end{aligned} \tag{2.108}$$

where a non-linear operator G is defined by

$$G(\Psi) = \hat{H}\Psi + \frac{i}{2}\sum_i \gamma_i ||\hat{A}_i\Psi||^2\Psi, \tag{2.109}$$

with the linear operator

$$\hat{H} = H - \frac{i}{2}\sum_i \gamma_i \hat{A}_i^\dagger \hat{A}_i. \tag{2.110}$$

Here, H describes the Hamiltonian of the Lindblad Eq. (2.98). The jump part is described by

$$\begin{aligned} \frac{\partial}{\partial t}\rho_{\mathrm{S}}\Big|_{\mathrm{J}} &= \int D\Psi D\Psi^* \int D\tilde{\Psi}D\tilde{\Psi}^*\Psi(x)\Psi^*(x')\left\{W[\Psi|\tilde{\Psi}]P[\tilde{\Psi},t] - W[\tilde{\Psi}|\Psi]P[\Psi,t]\right\} \\ &= \sum_i \gamma_i \hat{A}_i\rho_{\mathrm{S}}\hat{A}_i^\dagger - \sum_i E\left[||\hat{A}_i\Psi||^2\Psi(x)\Psi^*(x')\right]. \end{aligned} \tag{2.111}$$

When adding Eq. (2.108) and Eq. (2.111) the correlation terms of fourth order cancel and the quantum master Eq. (2.98) in Lindblad form is obtained. Hence, it is possible to circumvent the numerically expensive solution of the quantum master equation by describing the system's evolution by a PDP.
When unravelling the master equation with a PDP it is often more convenient to reformulate the propagation of the system by employing the stochastic variable $\Psi(t)$ itself, instead of the probability density. That leads to the stochastic differential equation

$$\mathrm{d}\Psi(t) = -iG\left(\Psi(t)\right)\mathrm{d}t + \sum_i \left(\frac{\hat{A}_i\Psi(t)}{||\hat{A}_i\Psi(t)||} - \Psi(t)\right)\mathrm{d}N_i(t), \tag{2.112}$$

where a discrete set of jumps, $\Psi(t) \to \frac{\hat{A}_i\Psi(t)}{||\hat{A}_i\Psi(t)||}$, is assumed to take place. It can be shown that Eq. (2.102) and a differential equation of the form in Eq. (2.112) lead to the same dynamical behaviour. In Eq. (2.112) the number of jumps for the ith transition in $\mathrm{d}t$ is denoted by $\mathrm{d}N_i(t)$ and obeys

$$E[\mathrm{d}N_i(t)] = \gamma_i(t)||\hat{A}_i\Psi(t)||^2\mathrm{d}t \tag{2.113}$$

$$\mathrm{d}N_i(t)\mathrm{d}N_j(t) = \delta_{ij}\mathrm{d}N_i(t). \tag{2.114}$$

Thus, for small $\mathrm{d}t$ the increments $\mathrm{d}N_i(t)$ behave like independent, inhomogeneous Poisson processes with transition rates $\gamma_i(t)$. According to Eq. (2.114) in a time $\mathrm{d}t$ either no jump occurs ($\mathrm{d}N_i(t) = 0\ \forall i$), or $\mathrm{d}N_i = 1$ for only one i and the remaining are zero. In the first case, only the first term in Eq. (2.112) appears and the system evolves deterministically. In the second case, a deterministic drift followed by a certain jump i takes place.
The probability for a jump to occur out of state Ψ in the interval $[t, t+\tau]$ is given by

$$F[\Psi, \tau] = 1 - ||e^{-i\hat{H}\tau}\Psi||^2, \tag{2.115}$$

where τ is the waiting time. According to Eq. (2.115) the jump probability is determined by the decrease of norm of the state obeying the linear part of Eq. (2.112).

2.3.4 Vibration-Electron coupling

One of the most important dissipative channels for adsorbates on metallic surfaces is the coupling of molecular vibrations to surface electrons. Due to the missing band gap in metallic systems the conduction electrons around the Fermi level can be excited resonantly by an arbitrarily low amount of energy, thus creating an electron-

hole pair.[28,43] The creation of such electron-hole pairs has a direct influence on the adsorbate dynamics since it leads to new electronic states and associated new potential energy surfaces which couple to each other. There are basically two coupling regimes depending on the electronic states involved: the strong and weak coupling limits. In order to understand both limits it is instructive to look at the molecular electronic states on the surface. If the molecular electronic states of the gas phase are embedded in the (quasi-)continuum of the conduction band they are shifted and lifetime broadened. In a good approximation the former discrete states can be described as bands. The coupling between states in different bands is called strong because the character of the wave function changes significantly when going from one wave function to another. Dynamics in the strong coupling regime are typically described by surface hopping methods, where the system is propagated classically and subjected to stochastic jumps between different PES.[81–83] However, for small amplitude motions around the equilibrium the fundamental band and the excited bands are well separated so that strong coupling can be neglected.
The weak coupling occurs between electronic states within a band and involves wave functions which are very similar in character. For classical nuclei $\{R_\alpha\}$ it can be shown that in the weak coupling limit their dynamical evolution can be described by a generalized Langevin equation[91–93]

$$m_\alpha \ddot{R}_\alpha = \bar{F}_\alpha - \sum_\nu \int_0^t \mathrm{d}t' \eta_{\alpha\nu}(t,t')\dot{R}_\nu(t') + \delta F_\alpha(t). \tag{2.116}$$

Eq. (2.116) describes a particle moving under an averaged force $\bar{F}_\alpha$ and a frictional force, described by the friction tensor $\eta_{\alpha\nu}$. In order to fulfil the equipartition theorem at finite temperature there is a fluctuating force δF_α obeying the fluctuation-dissipation theorem.[93] In many situations Eq. (2.116) can be simplified by assuming a Markovian system, i.e. $\eta_{\alpha\nu}(t,t') = \eta_{\alpha\nu}\delta(t-t')$. Besides, in the weak coupling regime the character of the electronic states is very similar, i.e. it is reasonable to assume PES which are parallel to each other. Thus, the averaged force is replaced by the force arising from the adiabatic ground state V. The final Langevin equation becomes,

$$m_\alpha \ddot{R}_\alpha = -\frac{\partial V}{\partial R_\alpha} - \sum_\nu \eta_{\alpha\nu}\dot{R}_\nu(t) + \delta F_\alpha(t). \tag{2.117}$$

Applying Eq. (2.117) in dynamical simulations is typically termed molecular dynamics with electronic friction (MDEF).
Dou *et al.* have given a general formula for the friction tensor but for most systems it is not feasible to explicitely calculate that expression.[92] Instead, there is a variety

of different friction models, e.g. jellium-based models,[131–133] orbital-dependent friction,[57,91,134] or models based on time-dependent DFT calculations.[135,136] Due to its simplicity, a very popular model is the local-density friction approximation (LDFA). In that model the friction tensor is diagonal with tensor elements

$$\eta_{\alpha\alpha}(\vec{R}) = \frac{3\hbar}{r_{\mathrm{S}}^2(\vec{R})}\left(\frac{4}{9\pi}\right)^{1/3}\sum_{l=0}^{\infty}(l+1)\sin^2[\delta_{l,\alpha}(r_{\mathrm{S}}) - \delta_{l+1,\alpha}(r_{\mathrm{S}})], \tag{2.118}$$

with the Wigner-Seitz radius r_{S}. The atoms are embedded in a free electron gas with embedding density $\rho_{\mathrm{emb}} = (\frac{4\pi}{3}r_{\mathrm{S}}^3)^{-1}$ and the frictional force is caused by a momentum transfer from the atoms to the metal electrons, resulting in a phase shift $\delta_{l,\alpha}$ of the Kohn-Sham orbitals.

In a classical description, the coupling to the electronic manifold of the surface results in a damping of the adsorbate motion. The strength, represented by the friction tensor, determines the damping rate of the total energy. In quantum mechanics the coupling of the system to the (electronic) environment induces transitions between the system's vibronic states with corresponding rates $\Gamma_{m\to n}$. Coupling between different vibronic states means it is necessary to go beyond the Born-Oppenheimer approximation. Usually, that is done by calculating the rates with first-order perturbation theory since the coupling between electronic states within a band is assumed to be weak. In the Born-Huang basis the resulting expression is

$$\begin{aligned}\Gamma_{m\to n} =& \frac{2\pi}{\hbar}\sum_{\alpha\beta}\left|\int \mathrm{d}\vec{R}\int \mathrm{d}\vec{r}\;\psi_n(\vec{R})\phi_\alpha(\vec{r};\vec{R})\hat{T}_{\mathrm{N}}\phi_\beta(\vec{r};\vec{R})\psi_m(\vec{R})\right|^2 \\ &\times f_\beta(E_\beta)(1-f_\alpha(E_\alpha))\delta(E_{\alpha,n}-E_{\beta,m}) \\ =& \frac{2\pi}{\hbar}\sum_{\alpha\beta}\left|\left\langle n\right|\left\langle \mathrm{e}_\alpha\right|\hat{T}_{\mathrm{N}}\left|\mathrm{e}_\beta\right\rangle\left|m\right\rangle\right|^2 f_\beta(E_\beta)(1-f_\alpha(E_\alpha))\delta(E_{\alpha,n}-E_{\beta,m}),\end{aligned} \tag{2.119}$$

with the Fermi-Dirac distribution f_α describing the electronic density of states and $|m\rangle$ and $|\mathrm{e}_\beta\rangle$ describing the nuclear and electronic wave functions. The above expression holds at 0 K, at finite temperatures the vibrational density of states has to be included by a Bose-Einstein factor.[137] In contrast to Eq. (2.17) the Born-Huang basis in Eq. (2.119) has different indices for electronic and vibrational states because they are assumed to be separable within a band. For the kinetic operator in Eq. (2.119) it is always possible to find a set of independent coordinates $\{q\}$ for which

$$\hat{T}_{\mathrm{N}} = -\frac{\hbar^2}{2}\sum_{q=1}^{3N}\frac{1}{M_q}\frac{\partial^2}{\partial q^2} = \sum_q \hat{T}^{(q)}. \tag{2.120}$$

By only considering first-order processes this leads to a summation of contributions $\Gamma^{(q)}_{m\to n}$ of $3N$ independent dissipation channels,

$$\Gamma_{m\to n} = \sum_q \Gamma^{(q)}_{m\to n}. \tag{2.121}$$

When neglecting higher-order terms[94,138,139] the corresponding matrix in Eq. (2.119) elements are given by

$$T^{(q)}_{\alpha\beta mn} = \frac{\hbar^2}{M_q} \langle n| \langle \mathrm{e}_\alpha| \frac{\partial}{\partial q} |\mathrm{e}_\beta\rangle \frac{\partial}{\partial q} |m\rangle . \tag{2.122}$$

The inner matrix element can be approximated by

$$\langle \mathrm{e}_\alpha| \frac{\partial}{\partial q} |\mathrm{e}_\beta\rangle = f(q) \langle \mathrm{e}_\alpha| \frac{\partial}{\partial q} |\mathrm{e}_\beta\rangle \Big|_{\mathrm{ref}}, \tag{2.123}$$

in order to fully separate electronic and vibrational coordinates.[140] That leads to

$$T^{(q)}_{\alpha\beta mn} = \frac{\hbar^2}{M_q} \langle \mathrm{e}_\alpha| \frac{\partial}{\partial q} |\mathrm{e}_\beta\rangle \Big|_{\mathrm{ref}} \langle n| f(q) \frac{\partial}{\partial q} |m\rangle . \tag{2.124}$$

Here, $f(q)$ scales the electronic contribution obtained at a reference position. When comparing the above expression to friction based models, e.g. LDFA, it appears physically reasonable to use the electronic embedding density to model $f(q)$,

$$f(q) = \rho^{1/3}_{\mathrm{emb}}(q). \tag{2.125}$$

The final rate expression is given by

$$\Gamma^{(q)}_{m\to n} = \frac{\zeta^{(q)}}{\omega_{mn}} | \langle n| \rho^{1/3}_{\mathrm{emb}} \frac{\partial}{\partial q} |m\rangle |^2, \tag{2.126}$$

where the scaling factor $\zeta^{(q)}$ contains the information about the momentum transfer between vibrations and electrons. It can be calculated explicitly depending on the chosen model or it is obtained by comparing Eq. (2.126) to a known rate. In general, the vibrational states in Eq. (2.126) are anharmonic. In the special case of harmonic states only one-quantum transitions are allowed, with a linear scaling of the rates,

$$\Gamma_{n\to n-1} = n\Gamma_{1\to 0}. \tag{2.127}$$

Apparently, the probability to relax in lower-lying states increases with the excitation of vibrational states. This trend is often even more pronounced for anharmonic eigenstates especially since they allow multi-quantum transitions.

Chapter 3

Summarized Results

The purpose of this thesis is to employ a quantum dynamical model to describe the scattering of NO from a Au(111) surface. In the last twenty years this system was extensively studied experimentally[12,59–62,66,67] and it is nowadays considered as the textbook example for the breakdown of the Born-Oppenheimer approximation at surfaces.[26,28] That system is chosen since the inclusion of the nonadiabatic character in the theoretical description is a challenging task but at the same time it promises a deeper understanding of many chemical and physical processes at metallic surfaces. The existing theoretical studies of the NO/Au(111) system still leave some questions open which are aimed to be adressed in this thesis.
This chapter recapitulates the results of the publications listed in Chapter 4 and illustrates the importance of a quantum dynamical description of scattering processes on metallic surfaces. It is organized along the three stages which were passed in order to study the NO/Au(111) system. The starting point is the construction of a new representation of the PES of the system and its spectroscopic characterization by an anharmonic eigenstate analysis (Sec. 3.1). Afterwards, in order to simulate the scattering in four dimensions at different surface sites a dissipative quantum dynamical model is developed and tested on its reliability (Sec. 3.2). In the last stage the newly constructed PES and the quantum model are combined to study the scattering dynamics of NO(ν=3) from Au(111) and these results are compared to MDEF simulations (Sec. 3.3).

3.1 Potential energy surface and spectroscopic analysis

In **Paper A** a new representation of the PES for the NO/Au(111) system in six dimensions is constructed. Previous quantum dynamical studies were based on two-dimensional PES resting upon *ab initio* calculations (periodic DFT[100]) or

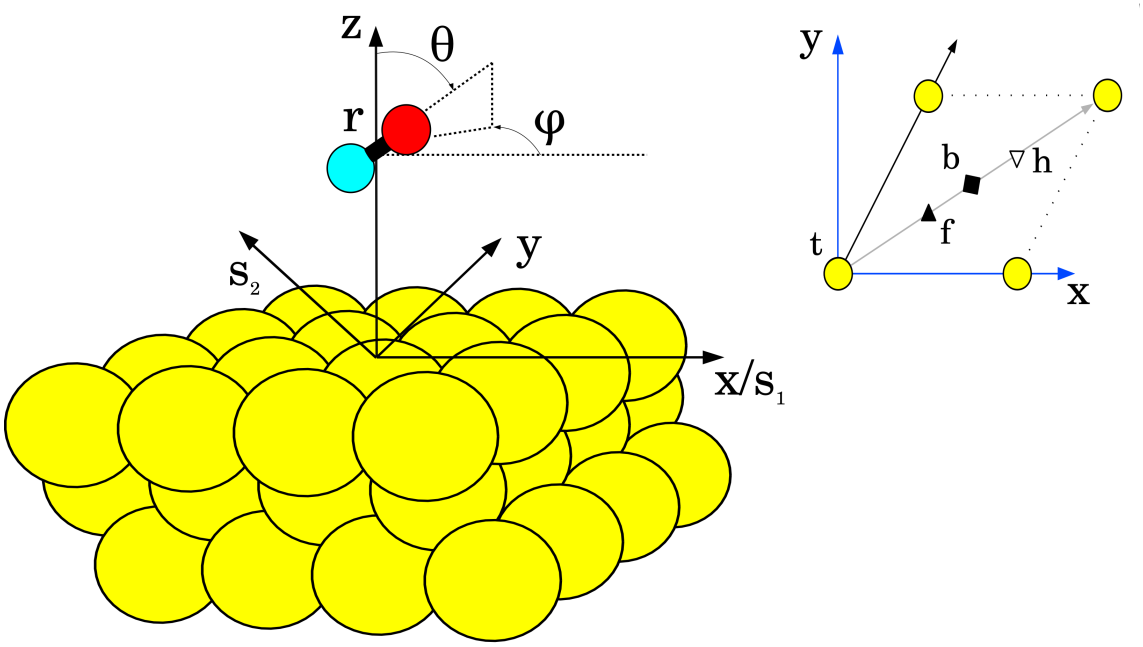

Figure 3.1: Definition of the coordinates (left panel) and surface sites (right panel) used in the construction of the PES. The configuration of the adsorbate is described by the cartesian coordinates of the center-of-mass given as $\{x, y, z\}$, the internal NO stretch coordinate as r, and the tilt and azimuthal angles as $\{\theta, \varphi\}$, respectively. Additionally, the axes along the skewed coordinates s_1 and s_2 are shown. The oxygen is depicted in red and the nitrogen in blue colour. The *ab initio* points were calculated at the top site (labelled "t"), the fcc hollow site (label "f", full triangle), the hcp hollow site (label "h", inverted empty triangle) as well as at the bridge site (label "b", full diamond). The figure is taken from **Paper A**.

semiempirical functions (two-state model[79]), where only the bond length r and the molecule-surface distance z were included. However, experimental findings imply an important role of the orientation of NO upon scattering by showing a clearly decreased relaxation probability for scattering with the oxygen pointing towards the surface.[66,67] Therefore, the aim is to characterize the potential energy landscape in full dimensions, i.e. including all six degrees of freedom by assuming a rigid surface (see Fig. 3.1). Tully and co-workers constructed such a six-dimensional PES for a diabatic two-state model[95] which was employed in several dynamical studies.[62,96–98] However, there are two reasons why we did not use that PES and decided to construct a new representation. First, the PES of Tully and co-workers completely neglects the top site of the (111) surface, whereas test calculations in the course of this thesis revealed the top site to be the most stable, in agreement with other periodic[141,142] as well as cluster[143–145] studies. Second, Tully *et al.* described the scattering dynamics in the strong-coupling limit (see Sec. 2.3.4), i.e. they used a diabatic two-state model including the ground states of the neutral and anionic diatomic, respectively. However, the quantum dynamical description envisaged in the later stage of this thesis is based on the weak coupling limit. As discussed in Sec. 2.3.4, the weak coupling limit only requires the adiabatic ground state onto which the system moves perturbed by the coupling to electron-hole pairs of the sur-

face. Thus, the new *ab initio* points are only calculated for the adiabatic ground state of neutral NO adsorbed on Au(111).

Periodic DFT (PW91) is chosen for these calculations since it is so far the only feasible method to calculate the large amount of points needed for a high-dimensional PES. Of course it would be desirable to employ a more accurate and systematically improvable electronic structure method. In particular, since it is known that for certain diatomics adsorbed on different metal surfaces current DFT functionals yield rather inaccurate adsorption energies[146] and for CO/Pt(111) they are not capable to reproduce the experimentally observed adsorption site.[147,148] Embedded cluster calculations employing accurate wave function based methods (CISD, CASSCF, CASPT2) are shown to yield good results[84–86] but aside from the large computational effort they demand a carefully chosen embedding technique.[87–90] Instead of using such a highly sophisticated embedding scheme we tried to improve upon the periodic DFT calculations by a subtractive scheme[149] where DFT and post-HF calculations on small clusters provide a correction which is then added to the periodic calculations. Cluster models of ten and six gold atoms were chosen to model top and hollow sites and a local coupled cluster method[150] was used to calculate accurate energies. Unfortunately, the unrestricted calculations (HF and DFT) suffered from a large spin contamination ($< \hat{S}^2 > \approx 1.4$). Restricted open-shell calculations were employed to clearly define the spin state and two electronic structure packages (Gaussian,[151] Molpro[152]) were tested. However, for the top-cluster the two programs did not produce the same results. At HF level, a ground state determinant was obtained with Gaussian but with Molpro the program always converged to an excited determinant. In addition, in subsequent calculations a T1 diagnostic around 0.03 (even > 0.04 in some regions) was observed indicating at least some multireference character. Due to these difficulties and the large computational time for the local coupled cluster calculations the idea of a correction term was abandoned and the PES was merely based on periodic DFT calculations.

These calculations are performed for NO at the three high symmetry sites as well as at the bridge site (see the right panel in Fig. 3.1). NO is found to favourably adsorb on top of a gold atom with an adsorption energy of $-373\,\mathrm{meV}$ which lies in the experimental range and indicates a weakly chemisorbed molecule.[153,154] On the top adsorption site the NO molecule is strongly tilted by $\sim 60^\circ$ since a back donation from the metal to the π^*-orbitals of NO takes place and the tilted configuration increases the overlap between the π^* orbitals and gold's d-orbitals. As will be disccused in Sec. 3.3 in more detail, this localization around $\sim 60^\circ$ will lead to a large population of rotational states which result in strongly enhanced relaxation rates (see Sec. 3.3). The adsorption at the hollow sites is found to be nearly 150 meV less favourable than atop and as expected, the structural and energetic

characteristics between fcc and hcp are rather similar. As for the top site, NO is tilted when adsorbing at the hollows, even though less strongly at ∼50°. For all adsorption sites the potential along the azimuthal angle φ was found to be almost barrierless, especially at the top site.

The calculated *ab initio* points are fitted to an analytical representation (SAP-PES) consisting of two- and three-body terms, originally developed by Marquardt *et al.*.[155] We choose that form since it is physically motivated and therefore correctly describes the system in the asymptotic limit. Besides, it allows a smaller set of points compared to numerical fitting strategies[156–164] since it reduces overfitting issues between the calculated points. The analytic form proposed by Marquardt *et al.* contains a switch function

$$p^{(3D)}(x,y,z) = p^{(\infty)} + (p^{(2D)}(x,y) - p^{(\infty)})(1 - e^{-(Z_s/z)^6}), \tag{3.1}$$

which describes the dependence of the parameters $\{p\}$ of the internal (Morse) potential with respect to the location of the NO on the surface. In the original work the switch function $p^{(2D)}$ was designed to incorporate the translational symmetry of a (100) surface. Hence, for the hexagonal gold surface a new form has to be found. However, a different approach was chosen after various attempts to design a new switch function $p^{(2D)}$ that correctly describes the translational symmetry along the surface and is flexible enough to describe the different sites. Instead of switching the parameters of the internal potential in a six-dimensional function a site-based strategy was employed where four dimensional potentials V_{4D}^{site} are fitted independently at all three high-symmetry sites and switch functions S_{site} interpolate between these four-dimensional potentials,

$$\begin{aligned} V^{6D} = [&V_{4D}^{top}(r, z_N, \theta, \varphi) S_{top}(x_N, y_N) + V_{4D}^{fcc}(r, z_N, \theta, \varphi) S_{fcc}(x_N, y_N) \\ &+ V_{4D}^{hcp}(r, z_N, \theta, \varphi) S_{hcp}(x_N, y_N)][S_{top}(x_N, y_N) + S_{fcc}(x_N, y_N) + S_{hcp}(x_N, y_N)]^{-1}. \end{aligned} \tag{3.2}$$

The potential is expressed by means of the cartesian coordinates of the nitrogen atom $\{x_N, y_N, z_N\}$. The parameters of the switch functions are determined by fitting the *ab initio* points at the bridge site to the form in Eq. (3.2). Apart from the site-based strategy and the switch function the original SAP-PES is further modified by adding an image-charge term to the four-dimensional potential which shall account for the charge transfer from the surface to the adsorbate. It is a physically motivated term to model the binding situation more realistically. As mentioned earlier, the binding is characterized by a π^*-backbonding, i.e. electron density of the metal is shifted in the π^*-orbitals of NO. Especially for the adsorption at the top

site that additional term improves the analytical description of the *ab initio* points which might indicate a partial charge transfer during the adsorption.
The final analytical representation of the PES is then investigated by a spectroscopical analysis in order to further characterize the static properties of the NO/Au(111) system. In the analysis of the anharmonic eigenstates two basic observations can be made. At first, an anharmonic character even for low-lying eigenstates is revealed. And second, there is a distinct coupling between different modes (intermode coupling, IMC). The IMC is found to be largely responsible for the observed anharmonicity, especially for higher-lying states. In principle, it does not have to be that way. It is possible to have an anharmonic system without IMC, e.g. by a set of independent Morse oscillators. Therefore, in order to see if the IMC is largely responsible for the anharmonicity the vibrational density of states (VDOS) of the fully coupled system is compared to the VDOS of a ficticious system of uncoupled Morse oscillators. The parameters of the latter are obtained by fits of the lower-lying states of the coupled system. That comparison shows a significantly larger increase in the VDOS for the coupled system compared to the uncoupled Morse oscillators demonstrating the strong effect of IMC on the anharmonicity of higher-lying vibrational states. The IMC of the system is further revealed by looking at the anharmonic eigenstates which cannot be characterized as pure overtones or combinational modes. Due to the IMC there is no possibility to use a coordinate transformation to uncouple the coordinates, i.e. the IMC is an intrinsic property and no artefact of the chosen coordinates. Whereas the IMC between the stretch coordinate r and the remaining degrees of freedom is rather weak, there is a significant coupling between the θ and z coordinate. The coupling between both coordinates supports the initial decision that an inclusion of the tilt angle in the PES is necessary for a correct description of the system. The later dynamical studies in Sec. 3.3 reveal the coupling to be vital for the relaxation process by providing more transfer channels for an energy redistribution within the system. The tilt angle θ as well as the z coordinate were also found to couple the translational degrees of freedom along the surface.

The structural properties of the NO/Au(111) system were observed to be quite sensitive with respect to the lattice constant. In **Paper A** the experimental lattice constant of 4.08 Å is employed in all calculations.[165] For that choice the adsorption of NO on the hollow sites is a transition state with a tilted NO rather high above the surface ($z_{\mathrm{surf-N}} \approx 2.9$ Å). In later work the lattice constant is relaxed with the same setup (functional, k-grid) adopted in **Paper A**. Even though the relaxation only increases the lattice constant by $\sim 2\,\%$ from 4.08 Å to 4.17 Å the NO adopts a perpendicular configuration at the hollow site at an equilibrium distance of $z_{\mathrm{surf-N}} \approx$ 1.8 Å. Now, the adsorption at the hollows describes a local minimum. For NO

adsorbed atop only very small changes were found when relaxing the lattice. Since we believe the perpendicular adsorption of NO on Au(111) to describe a physically more realistic situation, in which a π^*-backdonation from all three surrounding gold atoms contributes equally to the binding situation, the relaxed lattice constant is employed in the following. A perpendicular orientation is also in accordance with other comparable systems.[166] The *ab initio* points were recalculated with the relaxed lattice constant and refitted afterwards. This new representation is the basis for the following studies. It shows similar root-mean-square errors ($\sim 40\,\mathrm{meV}$ for energies up to $\sim 900\,\mathrm{meV}$ above the minimum) which demonstrates the high flexibility of the analytical form to adapt to different structural situations. Also the new fits of the hollow sites reveal a distinct IMC which can be seen in the potential itself which again shows coordinates that cannot be uncoupled by a coordinate transformation. Furthermore, the study presented in Section 3.3 also demonstrates the IMC by means of a strong energy transfer between the modes.

3.2 Quantum model

The second stage of this thesis is embarked upon in **Paper B** where a dynamical model is developed in order to describe the scattering process of diatomic molecules on metal surfaces in a quantum mechanical and dissipative fashion. For such scattering processes there are basically two dissipative channels: the coupling of molecular vibrations to electron-hole pairs and to phonons of the surface. The phononic channel was excluded in the following considerations since the experimental findings suggest a significant role of the former and only a minor importance of the latter,[59] at least for small-amplitude motion.[24] In order to have a computationally affordable model only the degrees of freedom which are most important for the dynamics should be included. Next to the center-of-mass coordinate z and the bond length r which were already used in previous studies, the orientational coordinates $\{\theta, \varphi\}$ are incorporated because, as already discussed in Sec. 3.1, there is a strong coupling between the tilt angle θ and the z coordinate (scattering coordinate). The $\{x, y\}$ coordinates which describe the lateral movement of the scatterer are not included in the dynamical model for two reasons. First, it is known from experiment that the scattering of NO from Au(111) is a direct process,[59] i.e. the NO molecule spends only a short time interval on the surface and thus diffusion is a negligible process. Second, the spectroscopic analysis in **Paper A** shows that there is a large VDOS of the lateral modes and the inclusion of that large amount of states would be computationally rather difficult to handle.

Typically, scattering processes on metal surfaces are performed by classical dynamics, e.g. by a Langevin equation which includes the coupling to electron-hole pairs

via an electronic friction tensor (see Eq. (2.117) in Chapter 2). However, such a description has proven itself insufficient to correctly describe the inelastic scattering of NO/Au(111) and the related vibrational relaxation.[65,98] A quantum dynamical treatment is promising since it can lead to increased dissipation rates, described by Eq. (2.126), which then result in stronger relaxation. The usual quantum dynamical approaches like surrogate Hamiltonians[167–169] or Multilayer MCTDH[76,170–172] are in the moment not suitable for dissipation to electron-hole pairs. Instead, in cases where that coupling shall be included the dynamic simulations are performed by means of density matrices,[100,173–175] typically in the weak coupling limit discussed in Chapter 2. However, a density matrix description in four dimensions with an unbound coordinate is computationally rather expensive due to the unfavourable scaling of $\mathcal{O}(N^3)$, with the dimension N of the Hilbert space.[176] Therefore, as discussed in more detail in Sec. 2.3.3 in Chapter 2, it is useful to unravel the quantum master equation for the density matrix by using a piecewise deterministic process. The overall procedure for the PDP used in this work is sketched in Fig. 3.2. In that approach a wave function is propagated deterministically for a certain time τ (step 1 in Fig. 3.2) after which it is decided (step 2 in Fig. 3.2) whether the wave packet is simply renormalized (step 3, right path in Fig. 3.2) or whether a stochastically chosen quantum jump occurs at the end of which the system is in a state localized near the surface (step 3, left path in Fig. 3.2). Such a stochastic approach is chosen for the quantum model in **Paper B**. For adsorbate/surface systems it was shown that the stochastic, wave function based approach converges to a density matrix solution with an affordable number of realizations,[177] i.e. number of independent wave function simulations. However, for the purposes of the inelastic scattering process considered in this thesis the usual stochastic propagation procedure is modified in two ways (see steps 2 and 4 in Fig. 3.2).

At first, a complex absorbing potential $W(z)$ (CAP[178]) along the scattering coordinate z is included in the deterministic propagation of the wave function in order to avoid artificial reflection of the wave packet arising from the finite grid. Often, these reflections are circumvented by very large grids which is however computational not feasible in the four-dimensional description. But avoiding the artificial reflection by using a CAP creates a new problem. As shown in Eq. (2.115) the probability of the wave packet to undergo a quantum jump is determined by the loss of norm caused by the dissipation operators in Eq. (2.97). If that loss is larger than a random number $\varepsilon \in [0, 1]$ a jump occurs, otherwise the wave packet is renormalized and propagated deterministically for a further time step. The larger the loss of norm the more likely a quantum jump occurs. Now, the CAP also decreases the norm which could lead to a quantum jump even if there is no effect of the dissipation operators. In order to avoid these unphysical jumps, the usual propagation procedure is modified (see

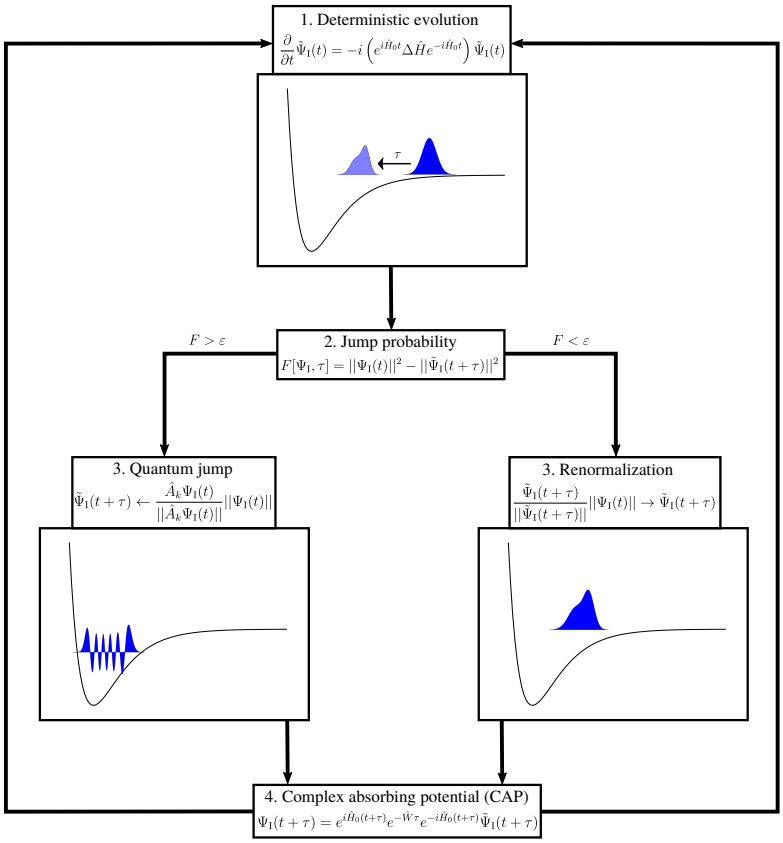

Figure 3.2: Pattern for the stochastic propagation scheme employed in **Paper B**. Step 1: the wave packet is propagated for a time step τ by a Schrödinger equation in the interaction picture (see **Paper B** for a detailed discussion of the partition of the Hamiltonian). Step 2: The jump probability (loss of norm) is determined and compared to a random number ε in order to decide whether a jump occurs or not. Step 3: Depending on the choice in step 2 the wave packet is simply renormalized (right path) or a specific dissipation channel k is stochastically chosen and the associated dissipation operator $\hat{A}_k$ acts on the wave packet (left pattern). This results in a wave function which is in a state of the relaxation basis. Step 4: A CAP acts on the wave packet and removes the parts of the wave packet which are near the right end of the z grid in the above picture. Afterwards the propagation starts again at step 1 and proceeds.

Fig. 3.2). A split-operator strategy is used, i.e. the CAP is applied not until the wave packet is propagated under the Hamiltonian without CAP and the decision concerning a jump is taken. This is reflected by step 4 in Fig. 3.2 which is newly introduced. When deciding if a jump occurs the jump probability in Eq. (2.115) has to be defined with respect to the norm a time step before (step 2 in Fig. 3.2) and the random numbers must be rescaled to that norm. Furthermore, after the decision whether a jump occurs or not the wave packet is renormalized with respect to the norm a time step before, otherwise the absorption of the wave packet at the previous time step would be reversed.

The second modification applies to the propagation and relaxation bases in which the system's Hamiltonian $\hat{H}_\mathrm{S}$ and the relaxation operators $\hat{A}_k$ are expressed. The natural choice for these representations is the basis of the fully-coupled eigenstates of $\hat{H}_\mathrm{S}$. However, this choice has certain drawbacks. Even though the fully-coupled basis is ideal to describe the system's evolution near the surface it is less suited further away. In this region a large number of eigenstates is necessary to obtain converged dynamics. In addition, extracting such a large number of multidimensional states is a numerically challenging task, especially if the system shows a strong IMC leading to high VDOS even at lower energies. Besides, for that large number of states the calculation of the associated transition rates by Eq. (2.126) constitutes an additional computational obstacle due the many multidimensional integrals that have to be calculated. For these reasons a different approach was employed in **Paper B**, where the propagation is described in a tensor product basis. Along the internal coordinates r and $\{\theta, \varphi\}$ Morse eigenstates and real spherical harmonics are used which shall mimic the experimentally observed rovibrational states in the gas phase. Along the scattering coordinate z a pseudospectral basis is chosen which enables a block diagonal form of the potential matrix and thus reduces the numerical cost for diagonalizing the Hamiltonian in the propagator.
Next, the basis for the relaxation operators has to be chosen. These operators are of the general form

$$\hat{A}_k = \hat{A}_{m\to n} = |n\rangle \langle m| \,. \tag{3.3}$$

After acting with $\hat{A}_k$ on the wave packet the system is in state $|n\rangle$ of the relaxation basis. The associated transition rates are calculated by Eq. (2.126) but the explicit calculation of the scaling factors $\zeta^{(q)}$ shall be avoided since it is a numerically quite demanding approach.[179] To circumvent that effort, the scaling factor for each mode q is obtained by comparing Eq. (2.126) to known fundamental rates $\Gamma^{(0)}_{1\to 0}$ which are calculated in the harmonic limit by means of the normal modes of the system.[180] Since the stochastic representation of the quantum master Eq. (2.98) by means of

a PDP is not unique a proper choice for the relaxation basis has to be made. In the present case that means that the relaxation basis has to resemble the normal modes. This basis directs the system towards the surface when a quantum jumps occurs. The chosen propagation basis does not fulfill this requirement. Therefore, a new basis in tensor product form is chosen for the relaxation. It consists of a one-dimensional basis $\{|\nu_z\rangle\}$ for the z mode and a three-dimensional basis $\{|i\rangle\}$ defining the internal modes r, θ, φ. The respective functions are the eigenstates of certain cuts of the PES which ensure the states to be localized near the surface. The associated relaxation rates have to vanish asymptotically since there is no coupling to electron-hole pairs far away from the surface. For the $\{|\nu_z\rangle\}$ basis that is accomplished by only considering bound states. That guarantees that the coupling to electron-hole pairs directs the wave packet towards the surface. In order to ensure asymptotically vanishing rates between the internal relaxation basis functions $\{|i\rangle\}$ these rates are scaled by the relative electron density., i.e. the electron density with respect to a reference position above the surface. Since the electron density is a measure for the electronic density of states near the Fermi level it is used to modulate the strength of the coupling to electron-hole pairs.

Based on that modified procedure, simulations in four dimensions are performed at a chosen $\{x, y\}$ location on the surface. After executing many of these wave function propagations (realizations) the desired expectation values are obtained by averaging over all realizations. Previous studies have demonstrated that it is possible to average over the expectation values obtained at many different surface sites to converge to observables of full-dimensional simulations.[181–184] In this thesis a site-average over the three high-symmetry sites (top, hcp, fcc) of the (111) surface is done. That is of course a rather coarse-grained average but it corresponds to the site-based strategy of the employed PES which is most trustworthy at these three sites (see Sec. 3.1).
In summary, compared to previous models the quantum model developed in **Paper B** is advanced in three ways:

- The orientational degrees of freedom $\{\theta, \varphi\}$ are included which allows a better consideration of IMC in the dynamics.

- A CAP is included and the propagation as well as the decision about quantum jumps are modified accordingly. By doing so unphysical interference effects due to the finite grid can be avoided. Besides, it allows a smaller grid for the propagation along z and thus decreases the computational effort significantly.

- A special relaxation basis is chosen which realistically models the vibrational states near the surface and yields reasonable relaxation rates. Hence it ensures

that the wave packet is directed towards the surface when it interacts with electron-hole pairs.

The constructed quantum dynamical model is tested upon its efficiency and physical soundness by performing some exemplary simulations with realistic initial conditions for the scattering of NO from Au(111) based on the PES constructed in **Paper A**. An essential criterion for the efficient application of the stochastic wave function based method compared to a density matrix approach is a small number of realizations. Convergence tests show that ~ 50 realizations are sufficient to converge the observables of interest, e.g. kinetic energies and expectation values of coordinates. For observables which are associated with more rare events, e.g. dissociation probabilities, the number of realizations needs to be higher but for observables like the final rotational and vibrational distribution the developed quantum model is an efficient alternative to a density matrix simulation.

Furthermore, the propagation is investigated in more detail to see the effect of the environment on the system's states and to understand in which circumstances the friction induced jumps occur. One effect caused by the coupling to electron-hole pairs is sticking or trapping, respectively. That describes a situation in which the scatterer loses enough momentum along z so that it cannot escape the surface region (sticking) or that it stays there for a considerable time (trapping). In a classical picture that corresponds to a particle bouncing back and forth multiple times on the surface. In a quantum mechanical friction picture sticking and trapping have their respective origin in wave packets which are projected onto a state near the surface or onto states with a small momentum along z (see the upper panel in Fig. 3.3). In both cases after averaging over many such realizations the resulting wave packet is more diffuse and at least parts of the wave packet stay considerably longer above the surface when compared to the adiabatic description. For the test system of NO/Au(111), without friction the wave packet stays a few hundred femtoseconds on the surface whereas with friction parts of the wave packet remain some picoseconds near the surface.

The effect of friction, i.e. the number of quantum jumps, is in general larger if the wave packet is closer to the surface due to the larger electron density which is connected to the coupling strength to electron-hole pairs. According to Eq. 2.126 a larger electron density increases the transition rate which increases the loss of norm and thus enhances the jump probability (see step 2 in Fig. 3.2). However, as exemplified in the upper panel of Fig. 3.3 jumps can also occur when the wave packet is farther away from the surface in regions of lower electron density, i.e. in regions where the coupling to electron-hole pairs is small and hence the single transition rates are small. That is because the decrease in norm caused by the non-hermitean term in the linear Hamiltonian in Eq. (2.110) depends on a sum over all transitions between

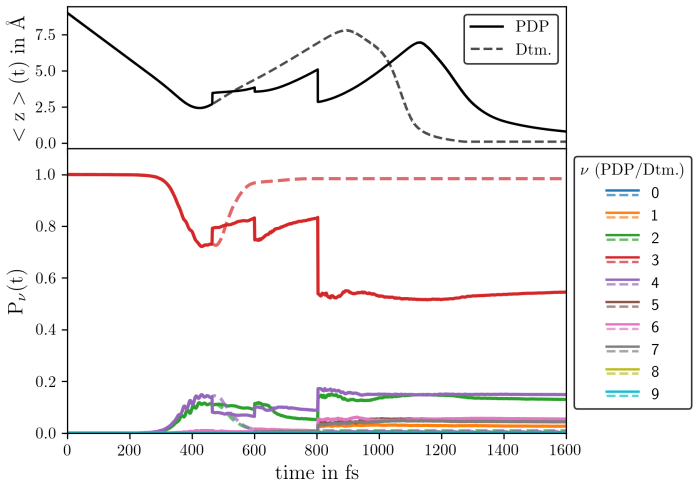

Figure 3.3: Upper panel: Expectation value of z in time for an exemplary realization with quantum jumps (solid line) and without jumps (dashed line). The labels PDP and Dtm stand for Piecewise Deterministic Process and Deterministic process, respectively. The decreasing curve at later time is due to the CAP because the shown expectation value only considers the part of the wave packet that is still in the box. Lower panel: Population of the asymptotic vibrational states integrated over z, θ and φ for a realization with quantum jumps (solid line) and without jumps (dashed line), respectively. The figure is taken from **Paper B**.

relaxation states. If many states are occupied there are many possible transitions. These transitions may have small rates but the sum over all these small contributions can lead to a non-negligible loss of norm and thus a finite jump probability. In the case of NO/Au(111) many rotational states are occupied, even farther away from the surface and these populated states can partially compensate for the smaller electronic density, i.e. the smaller coupling to electron-hole pairs. Additionally, that effect is amplified since the transition rates become larger the higher excited the states are (see the linear increase for the harmonic case in Eq. (2.127)).
Another friction-induced effect is vibrational relaxation. Without friction-induced quantum jumps the scattering of NO from Au(111) is vibrationally elastic. There are only rotational excitations caused by the strong IMC (see Sec. 3.1) which enables an internal energy transfer from translation to rotations. However, if quantum jumps are considered it happens that they lock population in propagation states which, in a purely adiabatic description, would decrease or increase upon their initial value (see Fig. 3.3 as an example of a realization with quantum jumps and without). That is crucial for the final vibrational distribution since at the expense of the initial vibrational state it allows an asymptotic population of states which are only transiently populated in an adiabatic simulation. In the chosen example of NO/Au(111) that leads to the population of the neighbouring states ($\nu = 2$

and $\nu = 4$). Interestingly, this shows that not only relaxation but also excitation is possible. From a classical point of view that seems counterintuitive since the friction tensor in the Langevin Eq. 2.117 leads to a damping force which drives the system to lower energies. In a quantum mechanical description relaxation as well as excitation are seen since on the surface the bond elongates and the initial vibrational state becomes a linear combination of several (lower- and higher-lying) basis states, which are defined with respect to the gas phase. If the population in these states is locked by the quantum jumps, as described above, many possible vibrational states, even excited ones, can be found in the final distribution. Accordingly, the population of excited states is slightly stronger for scattering at the hollow sites due to the stronger elongation of the bond caused by a deeper penetration of the surface.

All simulations performed in **Paper B** show the constructed quantum model to provide effects as sticking/trapping and vibrational relaxation which are also known from experiments for scattering dynamics on metal surfaces. In combination with the sufficiently small number of realizations to converge the considered observables the model provides a good and less expensive alternative to a density matrix description. Besides, the test simulations also show the constructed PES to be physically sound. Both, quantum model and PES are thus appropriate to be employed in a more systematic study of the scattering of NO from Au(111) in the following section.

3.3 Scattering of NO(ν=3) from Au(111)

In the last stage of this thesis, covered in **Paper C**, a detailed study of the scattering dynamics of NO($\nu = 3$) from a Au(111) surface with different initial translational energies is performed. For increasing initial kinetic energy along z experiments show a trend of increasing depopulation of the initial vibrational state ($\nu = 3$) and accordingly an increase of the population of $\nu = 2$ and $\nu = 1$[65] (see the black curve in Fig. 3.4). Previous classical and semiclassical studies[65,98] were not able to correctly reproduce that trend without imposing empirical constraints in their simulations.

The dynamical simulations in **Paper C** are done in four dimensions (r, z, θ, φ) at all three high-symmetry sites. For every observable of interest (branching ratio, population of rotational states and others) the average over all three sites (site-average) is taken in order to compare to experiment. This comparison is of course only approximate since a rather small number of positions along the surface is considered. However, the considered surface sites are sufficient to reproduce the experimental trend of increasing relaxation probability as a function of initial translational energy for state $\nu = 3$ (see Fig. 3.4). **Paper C** is the first theoretical work considering the coupling of molecular vibrations to electron-hole pairs that is able to reproduce

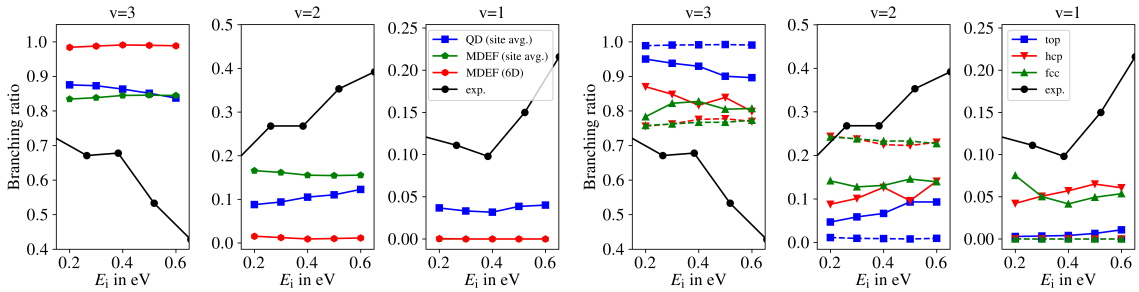

Figure 3.4: Branching ratio for scattering in vibrational states ν=1, 2, 3 at different initial translational energies. Values obtained from experiment are shown with black circles. Part a) shows site averaged quantum dynamics (QD, blue square), site averaged MDEF (green pentagon) and six-dimenional MDEF (red hexagon) simulations. Part b) shows reduced-dimensional simulations at top (blue square), hcp (red lower triangle) and fcc (green upper triangle). Site-averaged QD as solid lines and reduced-dimensional MDEF as dashed lines. The branching ratio in all figures is defined by means of the absolute state populations $P(\nu)$ as $P(\nu)/[P(\nu=1)+P(\nu=2)+P(\nu=3)]$. The figures are taken from **Paper C**.

this experimental trend. The agreement is qualitative, theory and experiment differ in absolute value as well as in the strenght of the trend. That might be due to a missing inclusion of surface phonons. In a classical study Yin *et al.* have recently shown that an explicit inclusion of surface motion in the adiabatic PES can account for a large part of vibrational relaxation.[99] An explicit treatment of surface phonons would not be feasible in the current quantum dynamical treatment but they could be included implicitly in the present model via an additional rate describing the phonon-induced transitions. Apart from further dissipation channels a full-dimensional treatment might also be essential for better agreement with experiment. The characterization of the PES in **Paper A** suggests an IMC between $\{x, y\}$ and z and θ which will probably lead to stronger energy redistribution by transfering energy in the lateral motion. The increased dimensionality would also lead to more relaxation and excitation channels which can contribute to the sum in Eq. (2.110) and the resulting enhanced dissipation could possibly lead to a stronger relaxation.

Already in the reduced-dimensional system the IMC is of large importance, namely for the distribution of rotational states. Especially at the top site the distribution shows a rotational rainbow, i.e. a large number of rotationally excited states which are populated. The distribution is broadened and shifted to higher energies when increasing the initial translational energy (see the upper panel of Fig. 3.5). While the former is a frictional effect the latter is founded in the potential's topology. The strong IMC between θ and z mode, observed and discussed in **Paper A**, en-

ables a strong energy transfer from translation to rotations and thus a population of many rotational states. In particular, for scattering at the top site the rotational rainbow is rather pronounced due to the strongly tilted orientation around $\theta \approx 60°$ (see Sec. 3.1). That is not surprising since the rotational degrees of freedom are described by spherical harmonics. The first spherical harmonic is a sphere and the lower-lying of these functions are mainly localized around $\theta = 0°$ and $\theta = 180°$, i.e. many spherical harmonics have to be populated to describe a wave packet localized around 60°. The coupling of molecular vibrations to electron-hole pairs enhances that primarily topological effect by excitations in higher-lying states. As already mentioned in Sec. 3.2 that effect is additionally supported since the transition rates become larger for higher excited states. At the hollow sites the NO is favourably adsorbed at 0°, accordingly the localization of the wave packet can be realized with a considerably smaller number of spherical harmoncis. That is indeed observed in the scattering simulations which show a less extensive rotational rainbow compared to the scattering at the top site. The rainbows and their shift with changing translational energy are in qualitative accordance with experimental findings. Thus, the PES and the quantum model developed in this thesis are able to confirm features of the rotations during the scattering process. A detailed comparison between experiment and simulations shows the latter to exaggerate the excitation of very high-lying rotational states ($j > 50$). This overestimation is probably due to the reduced dimensionality of the employed dynamical model. The translational energy is virtually exclusively transferred to rotations since in four dimensions there is no possibility for the molecule to move sideways and thus convert the translational energy into lateral motion.

Apart from the energy transfer within the system also a transfer from the molecular vibrations to the bath (electron-hole pairs) can be observed. A look at the system's total energy reveals a loss of energy which happens on a tens of picoseconds time scale. Interestingly, at the lowest initial translational energy ($E_i = 0.2\,\mathrm{eV}$) for the scattering at the top site the reduced-dimensional model even shows a gain in energy for the system. At first this seems surprising but it can be understood by a closer look at the microscopic processes. Every transition between two states of the relaxation basis has to obey detailed balance, the quotient of excitation and relaxation rate for every single transition is described by a Boltzmann distribution. Therefore, for a single transition at finite temperature relaxation rates are always larger than excitation rates. However, as discussed in Sec. 3.2 in the context of quantum jumps in regions of small electron-hole pair coupling (low density), the probability of a jump to occur depends on the sum over all possible transitions (channels). When many excited states are populated their large number can compensate the smaller excitation rates resulting in an excitation of the system. This overall excitation

is a temperature effect and vanishes at 0 K where only relaxation is present. The gain in total energy disappears for higher translational energies due to the shorter contact time on the surface. But at the top site there is still a visible competition between energy transfer from and to the system demonstrated by a minimum in the time-dependent total energy. Apparently, the model is able to account for an energy flow between system and bath in both directions. That energy transfer is mainly mediated by the scattering coordinate z, along which kinetic energy is lost, as known from experiments.[12] The initial kinetic energy is transferred to the bath as well as the rotations which is a further manifestation of the IMC found in **Paper A**. The energy along r is basically unaffected. For the vibrational coordinate r there is merely a conservative redistribution among the vibrational states visible in the rather symmetric distribution of the scattered molecule.

In theoretical surface science, as already mentioned in Sec. 3.2, MDEF simulations are the standard method for most dynamics studies, which consider electron-hole pairs, due to their low computational effort compared to quantum dynamical approaches. However, for most systems it is not clear whether a classical approach is justified. There are very little comparisons between classical and quantum dynamics for processes on surfaces.[185] In order to seize the opportunity for NO/Au(111) the constructed PES is also used to perform MDEF simulations which can be compared to the quantum dynamics discussed above. In a classical and a quantum picture the coupling of molecular vibrations to electron-hole pairs of the surface is described rather differently. As discussed in Sec. 2.3.4 of Chapter 2, in a classical treatment a frictional force damps the scatterer's motion. That is a continuous process with a single rate per mode. In contrast, discrete jumps are induced in the quantum picture with one rate for every pair of states. Besides, these rates are highly dependent on the anharmonic character and degree of excitation of the involved states. A direct comparison between MDEF simulations and the quantum model of **Paper B** may shed light on the importance of quantized relaxations in the dynamical description of scattering of NO from Au(111). And indeed, both descriptions differ quite substantially. Comparing the relaxation probabilities for different energies the absolute values are rather similar in the quantum and MDEF simulations in reduced dimensions at the respective sites (see Fig. 3.4b). However, the classical description shows a wrong trend, as also observed by Golibrzuch *et al.* for their PES,[65] i.e. the relaxation becomes less likely with increasing initial kinetic energy due to the smaller contact time on the surface. Yin *et al.* attribute the failure of MDEF to the potential representation and show that a high-dimensional PES including the surface atoms can yield the correct trend in a simple MD simulation. Even though an inclusion of surface motion may be desirable that does not degrade the finding that MDEF and QD do not yield a congruent dynamical description of

the scattering process since both are based on the PES of **Paper A**. A possible source of error is always the non-uniqueness of the friction tensor (see Sec. 2.3.4 in Chapter 2). In order to exclude that the results are an artefact of the chosen LDFA model (see Sec. 2.3.4 in Chapter 2) several MDEF simulations were performed in which the friction coefficients were increased by some factors since the chosen LDFA model is known to underestimate electronic friction.[133] The general trend is still wrong even when increasing the coefficients. Moreover, MDEF not only yields the wrong trend it shows only one-quantum relaxation in contrast to both experiment and quantum simulations (see Fig. 3.4). The quantum model is capable to describe also two-quantum relaxation since, as explained before in Sec. 3.2, on the surface along r the wave packet is a linear combination of many vibrational states in which the system can be locked by quantum jumps.

The fundamental difference between the quantum and classical description can be illustrated by the scattering from the top site. At that site the NO molecule is rather far away from the surface, i.e. the coupling to electron-hole pairs and thus the electronic density in that region is small. It is too small to create a significant frictional force in the Langevin equation (2.117) which would damp the molecule's motion in the MDEF simulation. In the quantum model the same electronic density is employed but, as mentioned earlier, the small individual transition rates in the regions of small density can be compensated by the high population of excited states along z and θ because the resulting large number of relaxation channels increases the influence of the dissipative term in Eq. (2.110). That effect becomes stronger for increasing initial kinetic energy because a) these populations increase with the kinetic energy along z and b) the respective transition rates become larger for higher-lying states. In contrast, for the MDEF simulations, the larger kinetic energy along z leads to a smaller contact time at the surface. Thus there is a smaller damping of the molecule's motion. Also the rotational distribution in Fig. 3.5 reveals discrepancies between MDEF and quantum simulations, especially at the top site. A rotational rainbow, i.e. excitation of many excited states, and a shift of the peaks with increasing kinetic energy can be seen in both simulations since as discussed before that is a topological effect and both methods are based on the same PES. In contrast, the broadening of the final rotational distributions is a frictional effect and is much more different when comparing both methods. In the quantum model the distribution broadens rather strongly with increasing kinetic energy whereas the MDEF simulations yield much more compact distributions. As discussed earlier, at the top site there is very little electronic density and thus only a minor classical, frictional effect. Therefore the rotational distribution is basically caused by the potential topology. In the quantum simulation the large number of relaxation and excitation channels increases the probability of quantum jumps which enables a

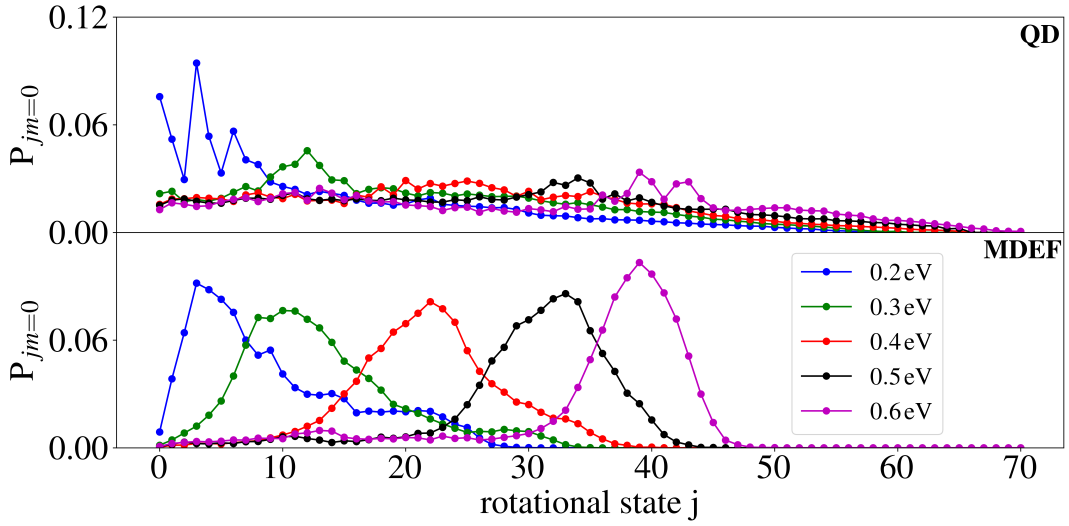

Figure 3.5: Population of the rotational states upon scattering at the top site at different initial kinetic energies. Top panel: quantum dynamics. Bottom panel: classical MDEF. The figure is taken from **Paper C**.

stronger deviation from a deterministic dynamic, i.e. a dynamic without quantum jumps. These quantum jumps lead to larger populations of states which results in the broadened distribution in the upper panel of Fig. 3.5. At the hollow sites the rotational distributions are more similar between both methods. That is because the localization of the wave packet around $\theta = 0°$ at the surface requires significantly less rotational states (spherical harmonics) than needed at the top site and the respective rates are smaller, as discussed earlier. Therefore less relaxation and excitation channels are available and there are less excited states which are likely to be populated by quantum jumps. Thus the deviation from the deterministic propagation, i.e. the propagation without quantum jumps, is less pronounced and the distributions resemble the rotational distributions of the MDEF simulations.
Of course, the differences for NO/Au(111) between classical (MDEF) simulations and the quantum dynamical model do not suspend classical methods when describing scattering dynamics, for system like H and H_2 scattering from various metals these methods are often rather successful.[186–188] But the differences emphasize that one has to be cautious when applying the MDEF approach to describe coupling to electron-hole pairs and that for some systems the inclusion of quantized relaxation might be essential to describe the main dynamical features correctly.

Chapter 4

Publications

The subsequent chapter presents the scientific publications which form the basis of this thesis. It contains three published works. For each of them, the contributions of the individual authors are outlined.

Paper A

"A new six-dimensional potential energy surface for NO/Au(111)"

T. Serwatka, B. Paulus and J. C. Tremblay

Mol. Phys. **117**, 42–57 (2019)
DOI: 10.1080/00268976.2018.1492041
URL: https://doi.org/10.1080/00268976.2018.1492041

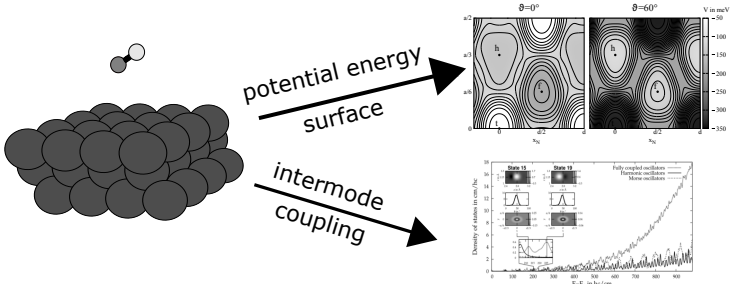

Graphical Abstract[A].()

Author contribution

The idea was conceived by Jean Christophe Tremblay. I did the test calculations with advice from Beate Paulus. The calculations of the final *ab initio* points and the fitting of these were done by me. The concept of the PES was developed by Jean Christophe Tremblay and myself. I calculated the anharmonic eigenstates with a program written by Jean Christophe Tremblay. The manuscript was mainly written by Jean Christophe Tremblay and myself with advice from Beate Paulus.

Paper B

"Stochastic wave packet approach to nonadiabatic scattering of diatomic molecules from metals"

T. Serwatka and J. C. Tremblay

J. Chem. Phys. **150**, 184105 (2019)
DOI: 10.1063/1.5092698
URL: https://doi.org/10.1063/1.5092698

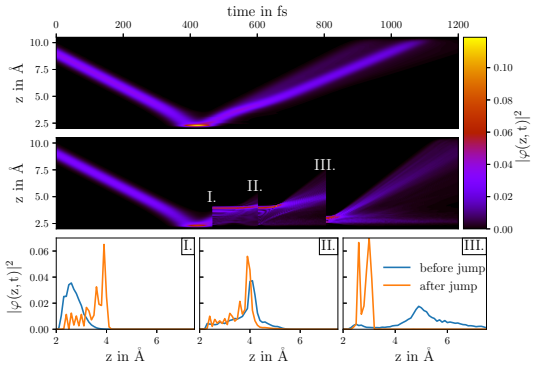

Figure taken from Paper B.(©2019 AIP Publishing LLC.)

Author contribution

The idea was conceived by Jean Christophe Tremblay. The quantum dynamical model was developed by Jean Christophe Tremblay and myself. I did the test simulations. Both authors contributed to the analysis. I wrote the manuscript with significant contributions from Jean Christophe Tremblay.

Paper C

"Scattering of NO(ν=3) from Au(111): a stochastic dissipative quantum dynamical perspective"

T. Serwatka, G. Füchsel and J. C. Tremblay

Phys. Chem. Chem. Phys. (2020), Advance Article
DOI: 10.1039/C9CP06084G
URL: https://doi.org/10.1039/C9CP06084G

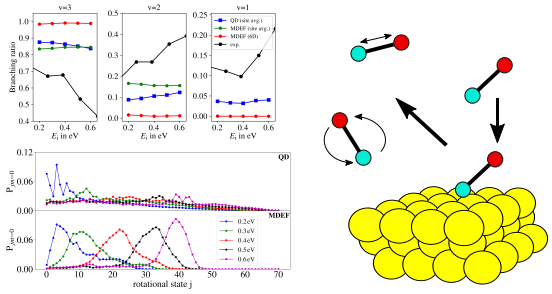

Graphical Abstract[C](©2020 Royal Society of Chemistry.)

Author contribution

The idea was conceived by Jean Christophe Tremblay and myself. I performed all quantum and classical calculations. The MDEF calculations were performed with a program written by Gernot Füchsel. The analysis was done by Jean Christophe Tremblay and myself. The manuscript was written by myself with contributions from Jean Christophe Tremblay and Gernot Füchsel.

Bibliography

(1) G. Ertl, *Angew. Chem.*, 1990, **102**, 1258–1266.

(2) R. Schlögl, *Angew. Chem. Int. Ed.*, 2003, **42**, 2004–2008.

(3) J. W. Erisman, M. A. Sutton, J. Galloway, Z. Klimont and W. Winiwarter, *Nat. Geosci.*, 2008, **1**, 636–639.

(4) G. P. Van Der Laan and A. Beenackers, *Catal. Rev. Sci. Eng.*, 1999, **41**, 255–318.

(5) B. H. Davis, *Fuel Process. Technol.*, 2001, **71**, 157–166.

(6) H. Mahmoudi, M. Mahmoudi, O. Doustdar, H. Jahangiri, A. Tsolakis, S. Gu and M. L. Wyszynski, *Biofuels Eng.*, 2017, **2**, 11–31.

(7) M. T. Koper, *Nanoscale*, 2011, **3**, 2054–2073.

(8) M. Zeng and Y. Li, *J. Mater. Chem. A*, 2015, **3**, 14942–14962.

(9) S. Zhang, Q. Fan, R. Xia and T. J. Meyer, *Acc. Chem. Res.*, 2020.

(10) G. Ertl, *Angew. Chem. Int. Ed.*, 2008, **47**, 3524–3535.

(11) S. P. Rittmeyer, V. J. Bukas and K. Reuter, *Adv. Phys. X*, 2018, **3**, 1381574.

(12) K. Golibrzuch, P. R. Shirhatti, J. Altschäffel, I. Rahinov, D. J. Auerbach, A. M. Wodtke and C. Bartels, *J. Phys. Chem. A*, 2013, **117**, 8750–8760.

(13) G. Lilienkamp and J. P. Toennies, *J. Chem. Phys.*, 1983, **78**, 5210–5224.

(14) P. Bratu and U. Höfer, *Phys. Rev. Lett.*, 1995, **74**, 1625.

(15) P. Kratzer, B. Hammer and J. K. Nørskov, *Phys. Rev. B*, 1995, **51**, 13432.

(16) I. Andrianov and P. Saalfrank, *J. Chem. Phys.*, 2006, **124**, 034710.

(17) B. D. Kay, T. Raymond and M. E. Coltrin, *Phys. Rev. Lett.*, 1987, **59**, 2792.

(18) M. Bonn, S. Funk, C. Hess, D. N. Denzler, C. Stampfl, M. Scheffler, M. Wolf and G. Ertl, *Science*, 1999, **285**, 1042–1045.

(19) R. Scholz, G. Floß, P. Saalfrank, G. Füchsel, I. Lončarić and J. Juaristi, *Phys. Rev. B*, 2016, **94**, 165447.

(20) K. Shakouri, J. Behler, J. Meyer and G.-J. Kroes, *J. Phys. Chem. Lett.*, 2017, **8**, 2131–2136.

(21) Q. Ran, D. Matsiev, A. M. Wodtke and D. J. Auerbach, *Rev. Sci. Instrum.*, 2007, **78**, 104104.

(22) Q. Ran, D. Matsiev, D. J. Auerbach and A. M. Wodtke, *Phys. Rev. Lett.*, 2007, **98**, 237601.

(23) J. C. Tully, *Ann. Rev. Phys. Chem.*, 2000, **51**, 153–178.

(24) A. M. Wodtke, J. C. Tully and D. J. Auerbach, *Int. Rev. Phys. Chem.*, 2004, **23**, 513–539.

(25) A. M. Wodtke, D. Matsiev and D. J. Auerbach, *Prog. Surf. Sci.*, 2008, **83**, 167–214.

(26) I. Rahinov, R. Cooper, D. Matsiev, C. Bartels, D. J. Auerbach and A. M. Wodtke, *Phys. Chem. Chem. Phys.*, 2011, **13**, 12680–12692.

(27) C. Bartels, R. Cooper, D. J. Auerbach and A. M. Wodtke, *Chem. Sci.*, 2011, **2**, 1647–1655.

(28) A. M. Wodtke, *Chem. Soc. Rev.*, 2016, **45**, 3641–3657.

(29) C. T. Rettner, F. Fabre, J. Kimman and D. J. Auerbach, *Phys. Rev. Lett.*, 1985, **55**, 1904.

(30) C. T. Rettner, J. Kimman, F. Fabre, D. J. Auerbach and H. Morawitz, *Surf. Sci.*, 1987, **192**, 107–130.

(31) T. Schäfer, N. Bartels, K. Golibrzuch, C. Bartels, H. Köckert, D. J. Auerbach, T. N. Kitsopoulos and A. M. Wodtke, *Phys. Chem. Chem. Phys.*, 2013, **15**, 1863–1867.

(32) J. Werdecker, P. R. Shirhatti, K. Golibrzuch, C. Bartels, A. M. Wodtke and D. J. Harding, *J. Phys. Chem. C*, 2015, **119**, 14722–14727.

(33) J. Geweke, P. R. Shirhatti, I. Rahinov, C. Bartels and A. M. Wodtke, *J. Chem. Phys.*, 2016, **145**, 054709.

(34) B. C. Krüger, S. Meyer, A. Kandratsenka, A. M. Wodtke and T. Schäfer, *J. Phys. Chem. Lett.*, 2016, **7**, 441–446.

(35) M. Pavanello, D. J. Auerbach, A. M. Wodtke, M. Blanco-Rey, M. Alducin and G.-J. Kroes, *J. Phys. Chem. Lett.*, 2013, **4**, 3735–3740.

(36) M. Blanco-Rey, J. Juaristi, R. D. Muiño, H. F. Busnengo, G.-J. Kroes and M. Alducin, *Phys. Rev. Lett.*, 2014, **112**, 103203.

(37) G.-J. Kroes, M. Pavanello, M. Blanco-Rey, M. Alducin and D. J. Auerbach, *J. Chem. Phys.*, 2014, **141**, 054705.

(38) P. Saalfrank, J. Juaristi, M. Alducin, M. Blanco-Rey and R. D. Muiño, *J. Chem. Phys.*, 2014, **141**, 234702.

(39) S. M. Janke, D. J. Auerbach, A. M. Wodtke and A. Kandratsenka, *J. Chem. Phys.*, 2015, **143**, 124708.

(40) O. Bünermann, H. Jiang, Y. Dorenkamp, A. Kandratsenka, S. M. Janke, D. J. Auerbach and A. M. Wodtke, *Science*, 2015, **350**, 1346–1349.

(41) Y. Dorenkamp, H. Jiang, H. Köckert, N. Hertl, M. Kammler, S. M. Janke, A. Kandratsenka, A. M. Wodtke and O. Bünermann, *J. Chem. Phys.*, 2018, **148**, 034706.

(42) H. Nienhaus, H. Bergh, B. Gergen, A. Majumdar, W. H. Weinberg and E. W. McFarland, *J. Vac. Sci. Technol. A*, 1999, **17**, 1683–1687.

(43) H. Nienhaus, *Surf. Sci. Rep.*, 2002, **45**, 1–78.

(44) E. Hasselbrink, *Curr. Opin. Solid State Mater. Sci.*, 2006, **10**, 192–204.

(45) D. Diesing and E. Hasselbrink, *Chem. Soc. Rev.*, 2016, **45**, 3747–3755.

(46) J. D. White, J. Chen, D. Matsiev, D. J. Auerbach and A. M. Wodtke, *Nature*, 2005, **433**, 503–505.

(47) J. L. LaRue, J. D. White, N. H. Nahler, Z. Liu, Y. Sun, P. A. Pianetta, D. J. Auerbach and A. M. Wodtke, *J. Chem. Phys.*, 2008, **129**, 024709.

(48) N. Nahler, J. White, J. L. LaRue, D. J. Auerbach and A. M. Wodtke, *Science*, 2008, **321**, 1191–1194.

(49) J. L. LaRue, T. Schäfer, D. Matsiev, L. Velarde, N. H. Nahler, D. J. Auerbach and A. M. Wodtke, *Phys. Chem. Chem. Phys.*, 2011, **13**, 97–99.

(50) J. L. LaRue, T. Schäfer, D. Matsiev, L. Velarde, N. H. Nahler, D. J. Auerbach and A. M. Wodtke, *J. Phys. Chem. A*, 2011, **115**, 14306–14314.

(51) C. Hirschmugl, G. Williams, F. Hoffmann and Y. Chabal, *J. Electron Spectrosc. Relat. Phenom.*, 1990, **54**, 109–114.

(52) J. Beckerle, M. Casassa, R. Cavanagh, E. Heilweil and J. Stephenson, *Phys. Rev. Lett.*, 1990, **64**, 2090.

(53) M. Morin, N. J. Levinos and A. L. Harris, *J. Chem. Phys.*, 1992, **96**, 3950–3956.

(54) B. N. J. Persson and M. Persson, *Solid State Commun.*, 1980, **36**, 175–179.

(55) J. C. Tully, M. Gomez and M. Head-Gordon, *J. Vac. Sci. Technol. A*, 1993, **11**, 1914–1920.

(56) V. Krishna and J. C. Tully, *J. Chem. Phys.*, 2006, **125**, 054706.

(57) M. Askerka, R. J. Maurer, V. S. Batista and J. C. Tully, *Phys. Rev. Lett.*, 2016, **116**, 217601.

(58) H.-C. Chang and G. E. Ewing, *Phys. Rev. Lett.*, 1990, **65**, 2125.

(59) Y. Huang, C. T. Rettner, D. J. Auerbach and A. M. Wodtke, *Science*, 2000, **290**, 111–114.

(60) R. Cooper, I. Rahinov, Z. Li, D. Matsiev, D. J. Auerbach and A. M. Wodtke, *Chem. Sci.*, 2010, **1**, 55–61.

(61) D. Matsiev, Z. Li, R. Cooper, I. Rahinov, C. Bartels, D. J. Auerbach and A. M. Wodtke, *Phys. Chem. Chem. Phys.*, 2011, **13**, 8153–8162.

(62) R. Cooper, C. Bartels, A. Kandratsenka, I. Rahinov, N. Shenvi, K. Golibrzuch, Z. Li, D. J. Auerbach, J. C. Tully and A. M. Wodtke, *Angew. Chem.*, 2012, **124**, 5038–5042.

(63) G. A. Gates, G. R. Darling and S. Holloway, *J. Chem. Phys.*, 1994, **101**, 6281–6288.

(64) Z. S. Wang, G. R. Darling and S. Holloway, *J. Chem. Phys.*, 2004, **120**, 2923–2933.

(65) K. Golibrzuch, P. R. Shirhatti, I. Rahinov, A. Kandratsenka, D. J. Auerbach, A. M. Wodtke and C. Bartels, *J. Chem. Phys.*, 2014, **140**, 044701.

(66) N. Bartels, K. Golibrzuch, C. Bartels, L. Chen, D. J. Auerbach, A. M. Wodtke and T. Schäfer, *Proc. Natl. Acad. Sci. USA*, 2013, **110**, 17738–17743.

(67) N. Bartels, K. Golibrzuch, C. Bartels, L. Chen, D. J. Auerbach, A. M. Wodtke and T. Schäfer, *J. Chem. Phys.*, 2014, **140**, 054710.

(68) M. Bonfanti, C. Díaz, M. F. Somers and G.-J. Kroes, *Phys. Chem. Chem. Phys.*, 2011, **13**, 4552–4561.

(69) D. Novko, M. Blanco-Rey, J. I. Juaristi and M. Alducin, *Phys. Rev. B*, 2015, **92**, 201411.

(70) K. Shakouri, J. Behler, J. Meyer and G.-J. Kroes, *J. Phys. Chem. C*, 2018, **122**, 23470–23480.

(71) S. Adelman and J. Doll, *J. Chem. Phys.*, 1976, **64**, 2375–2388.

(72) J. C. Tully, *J. Chem. Phys.*, 1980, **73**, 1975–1985.

(73) J. Polanyi and R. Wolf, *J. Chem. Phys.*, 1985, **82**, 1555–1566.

(74) H. F. Busnengo, W. Dong and A. Salin, *Phys. Rev. Lett.*, 2004, **93**, 236103.

(75) L. Martin-Gondre, M. Alducin, G. A. Bocan, R. D. Muiño and J. I. Juaristi, *Phys. Rev. Lett.*, 2012, **108**, 096101.

(76) Q. Meng and H.-D. Meyer, *J. Chem. Phys.*, 2017, **146**, 184305.

(77) P. Saalfrank, *Chem. Rev.*, 2006, **106**, 4116.

(78) J. Gadzuk, L. Richter, S. Buntin, D. King and R. Cavanagh, *Surf. Sci.*, 1990, **235**, 317–333.

(79) S. Li and H. Guo, *J. Chem. Phys.*, 2002, **117**, 4499–4508.

(80) N. Shenvi, S. Roy, P. Parandekar and J. Tully, *J. Chem. Phys.*, 2006, **125**, 154703.

(81) J. C. Tully, *J. Chem. Phys.*, 1990, **93**, 1061–1071.

(82) U. Müller and G. Stock, *J. Chem. Phys.*, 1997, **107**, 6230–6245.

(83) N. Shenvi, S. Roy and J. C. Tully, *J. Chem. Phys.*, 2009, **130**, 174107.

(84) F. Libisch, J. Cheng and E. A. Carter, *Z. Phys. Chem.*, 2013, **227**, 1455–1466.

(85) S. Mukherjee, F. Libisch, N. Large, O. Neumann, L. V. Brown, J. Cheng, J. B. Lassiter, E. A. Carter, P. Nordlander and N. J. Halas, *Nano Lett.*, 2013, **13**, 240–247.

(86) S. Sharifzadeh, P. Huang and E. Carter, *J. Phys. Chem. C*, 2008, **112**, 4649–4657.

(87) P. Huang and E. A. Carter, *J. Chem. Phys.*, 2006, **125**, 084102.

(88) C. Huang, M. Pavone and E. A. Carter, *J. Chem. Phys.*, 2011, **134**, 154110.

(89) C. Huang and E. A. Carter, *J. Chem. Phys.*, 2011, **135**, 194104.

(90) F. Libisch, C. Huang and E. A. Carter, *Acc. Chem. Res.*, 2014, **47**, 2768–2775.

(91) M. Head-Gordon and J. C. Tully, *J. Chem. Phys.*, 1995, **103**, 10137–10145.

(92) W. Dou, G. Miao and J. E. Subotnik, *Phys. Rev. Lett.*, 2017, **119**, 046001.

(93) W. Dou and J. E. Subotnik, *J. Chem. Phys.*, 2018, **148**, 230901.

(94) M. Head-Gordon and J. C. Tully, *J. Chem. Phys.*, 1992, **96**, 3939–3949.

(95) S. Roy, N. A. Shenvi and J. C. Tully, *J. Chem. Phys.*, 2009, **130**, 174716.

(96) N. Shenvi, S. Roy and J. C. Tully, *Science*, 2009, **326**, 829–832.

(97) K. Golibrzuch, A. Kandratsenka, I. Rahinov, R. Cooper, D. J. Auerbach, A. M. Wodtke and C. Bartels, *J. Phys. Chem. A*, 2013, **117**, 7091–7101.

(98) B. C. Krüger, N. Bartels, C. Bartels, A. Kandratsenka, J. C. Tully, A. M. Wodtke and T. Schäfer, *J. Phys. Chem. C*, 2015, **119**, 3268–3272.

(99) R. Yin, Y. Zhang and B. Jiang, *J. Phys. Chem. Lett.*, 2019, **10**, 5969–5974.

(100) S. Monturet and P. Saalfrank, *Phys. Rev. B*, 2010, **82**, 075404.

(101) D. J. Tannor, *Introduction to Quantum Mechanics: A time-dependent perspective*, University Science Books, 2007.

(102) W. Nolting, *Grundkurs Theoretische Physik 5/1, Quantenmechanik - Grundlagen*, Springer Spektrum, Berlin/Heidelberg, 2013.

(103) E. Schrödinger, *Ann. Phys.*, 1926, **384**, 361–376.

(104) M. Born and J. R. Oppenheimer, *Ann. Phys.*, 1927, **389**, 457–484.

(105) F. Jensen, *Introduction to Computational Chemistry*, John Wiley & Sons Ltd, 2007.

(106) A. Szabo and N. S. Ostlund, *Modern Quantum Chemistry: Introduction to Advanced Electronic Structure Theory*, Dover Publications Inc., New York, 1996.

(107) W. Koch and M. C. Holthausen, *A Chemist's Guide to Density Functional Theory*, Wiley-VCH Verlag GmbH, Weinheim, 2001.

(108) A. N. W. and D. N. Mermin, *Festkörperphysik*, Oldenbourg Verlag, München, 2013.

(109) C. C. J. Roothaan, *Rev. Mod. Phys.*, 1951, **23**, 69.

(110) G. G. Hall, *Proc. R. Soc. Lon. A.*, 1951, **205**, 541–552.

(111) T. Helgaker, P. Jørgensen and J. Olsen, *Molecular electronic-structure theory*, John Wiley & Sons, 2014.

(112) L. H. Thomas, Math. Proc. Camb. Philos. Soc. 1927, vol. 23, pp. 542–548.

(113) E. Fermi, *Rend. Accad. Lincei*, 1927, **6**, 602–607.

(114) P. Hohenberg and W. Kohn, *Phys. Rev.*, 1964, **136**, B864.

(115) W. Kohn and L. J. Sham, *Phys. Rev.*, 1965, **140**, A1133.

(116) W. J. Carr Jr., *Phys. Rev.*, 1961, **122**, 1437.

(117) W. J. Carr Jr. and A. A. Maradudin, *Phys. Rev.*, 1964, **133**, A371.

(118) S. H. Vosko, L. Wilk and M. Nusair, *Can. J. Phys.*, 1980, **58**, 1200–1211.

(119) J. P. Perdew, K. Burke and M. Ernzerhof, *Phys. Rev. Lett.*, 1996, **77**, 3865.

(120) A. D. Becke, *J. Chem. Phys.*, 1993, **98**, 1372–1377.

(121) A. D. Becke, *J. Chem. Phys.*, 1993, **98**, 5648–5652.

(122) P. J. Stephens, F. Devlin, C. Chabalowski and M. J. Frisch, *J. Phys. Chem.*, 1994, **98**, 11623–11627.

(123) J. Heyd, G. E. Scuseria and M. Ernzerhof, *J. Chem. Phys.*, 2003, **118**, 8207–8215.

(124) J. P. Perdew, M. Ernzerhof and K. Burke, *J. Chem. Phys.*, 1996, **105**, 9982–9985.

(125) C. Adamo and V. Barone, *J. Chem. Phys.*, 1999, **110**, 6158–6170.

(126) S. Grimme, J. Antony, S. Ehrlich and H. Krieg, *J. Chem. Phys.*, 2010, **132**, 154104.

(127) F. Bloch, *Z. Phys.*, 1929, **52**, 555–600.

(128) H.-P. Breuer and F. Petruccione, *The Theory of Open Quantum Systems*, Oxford University Press, Oxford, 2010.

(129) R. Zwanzig, *Nonequilibrium Statistical Mechanics*, Oxford University Press, New York, 2001.

(130) *Chemical Modelling, Volume 12*, ed. M. Springborg and J.-O. Joswig, Royal Society of Chemistry, Cambridge, 2015.

(131) E. G. d'Agliano, P. Kumar, W. Schaich and H. Suhl, *Phys. Rev. B*, 1975, **11**, 2122.

(132) M. J. Puska and R. M. Nieminen, *Phys. Rev. B*, 1983, **27**, 6121.

(133) S. P. Rittmeyer, J. Meyer, J. I. Juaristi and K. Reuter, *Phys. Rev. Lett.*, 2015, **115**, 046102.

(134) R. J. Maurer, M. Askerka, V. S. Batista and J. C. Tully, *Phys. Rev. B*, 2016, **94**, 115432.

(135) M. Timmer and P. Kratzer, *Phys. Rev. B*, 2009, **79**, 165407.

(136) J. Meyer and K. Reuter, *New. J. Phys.*, 2011, **13**, 085010.

(137) J. C. Tremblay, *J. Chem. Phys.*, 2013, **138**, 244106.

(138) G. P. Brivio and T. B. Grimley, *J. Phys. C: Solid St. Phys.*, 1977, **10**, 2351.

(139) G. P. Brivio and T. B. Grimley, *Surf. Sci.*, 1979, **89**, 226–237.

(140) J. C. Tremblay and P. Saalfrank, *J. Chem. Phys.*, 2009, **131**, 084716.

(141) W. Zhang, Z. Li, Y. Luo and J. Yang, *J. Chem. Phys.*, 2008, **129**, 134708.

(142) Y. Santiago-Rodriguez, J. A. Herron, M. C. Curet-Arana and M. Mavrikakis, *Surf. Sci.*, 2014, **627**, 57–69.

(143) X. Ding, Z. Li, J. Yang, J. Hou and Q. Zhu, *J. Chem. Phys.*, 2004, **121**, 2558–2562.

(144) A. Endou, N. Ohashi, S. Takami, M. Kubo, A. Miyamoto and E. Broclawik, *Top. Catal.*, 2000, **11**, 271–278.

(145) O. Olvera-Neria, V. Bertin and E. Poulain, *Int. J. Quantum Chem.*, 2011, **111**, 2054–2063.

(146) P. S. Schmidt and K. S. Thygesen, *J. Phys. Chem. C*, 2018, **122**, 4381–4390.

(147) P. J. Feibelman, B. Hammer, J. K. Nørskov, F. Wagner, M. Scheffler, R. Stumpf, R. Watwe and J. Dumesic, *J. Phys. Chem. B*, 2001, **105**, 4018–4025.

(148) L. Schimka, J. Harl, A. Stroppa, A. Grüneis, M. Marsman, F. Mittendorfer and G. Kresse, *Nat. Mater.*, 2010, **9**, 741–744.

(149) C. Tuma and J. Sauer, *Chem. Phys. Lett.*, 2004, **387**, 388–394.

(150) H.-J. Werner and M. Schütz, *J. Chem. Phys.*, 2011, **135**, 144116.

(151) M. J. Frisch, G. W. Trucks, H. B. Schlegel, G. E. Scuseria, M. A. Robb, J. R. Cheeseman, G. Scalmani, V. Barone, G. A. Petersson, H. Nakatsuji, X. Li, M. Caricato, A. V. Marenich, J. Bloino, B. G. Janesko, R. Gomperts, B. Mennucci, H. P. Hratchian, J. V. Ortiz, A. F. Izmaylov, J. L. Sonnenberg, D. Williams-Young, F. Ding, F. Lipparini, F. Egidi, J. Goings, B. Peng, A. Petrone, T. Henderson, D. Ranasinghe, V. G. Zakrzewski, J. Gao, N. Rega, G. Zheng, W. Liang, M. Hada, M. Ehara, K. Toyota, R. Fukuda, J. Hasegawa, M. Ishida, T. Nakajima, Y. Honda, O. Kitao, H. Nakai, T. Vreven, K. Throssell, J. A. Montgomery, Jr., J. E. Peralta, F. Ogliaro, M. J. Bearpark, J. J. Heyd, E. N. Brothers, K. N. Kudin, V. N. Staroverov, T. A. Keith, R. Kobayashi, J. Normand, K. Raghavachari, A. P. Rendell, J. C. Burant, S. S. Iyengar, J. Tomasi, M. Cossi, J. M. Millam, M. Klene, C. Adamo, R. Cammi, J. W. Ochterski, R. L. Martin, K. Morokuma, O. Farkas, J. B. Foresman and D. J. Fox, *Gaussian 16 Revision A.03*, Gaussian Inc. Wallingford CT, see https://gaussian.com/ (accessed Mar 8, 2020), 2016.

(152) H.-J. Werner, P. J. Knowles, G. Knizia, F. R. Manby, M. Schütz, P. Celani, W. Györffy, D. Kats, T. Korona, R. Lindh, A. Mitrushenkov, G. Rauhut, K. R. Shamasundar, T. B. Adler, R. D. Amos, S. J. Bennie, A. Bernhardsson, A. Berning, D. L. Cooper, M. J. O. Deegan, A. J. Dobbyn, F. Eckert, E. Goll, C. Hampel, A. Hesselmann, G. Hetzer, T. Hrenar, G. Jansen, C. Köppl, S. J. R. Lee, Y. Liu, A. W. Lloyd, Q. Ma, R. A. Mata, A. J. May, S. J. McNicholas, W. Meyer, T. F. Miller III, M. E. Mura, A. Nicklass, D. P. O'Neill, P. Palmieri, D. Peng, K. Pflüger, R. Pitzer, M. Reiher, T. Shiozaki, H. Stoll, A. J. Stone, R. Tarroni, T. Thorsteinsson, M. Wang and M. Welborn, *MOLPRO, version 2015.1, A Package of Ab Initio Programs*, see https://www.molpro.net/ (accessed Mar 8, 2020), 2015.

(153) S. M. McClure, T. S. Kim, J. D. Stiehl, P. L. Tanaka and C. B. Mullins, *J. Phys. Chem. B*, 2004, **108**, 17952–17958.

(154) D. P. Engelhart, R. J. Wagner, A. Meling, A. M. Wodtke and T. Schäfer, *Surface Science*, 2016, **650**, 11–16.

(155) R. Marquardt, F. Cuvelier, R. A. Olsen, E. J. Baerends, J. C. Tremblay and P. Saalfrank, *J. Chem. Phys.*, 2010, **132**, 074108.

(156) H. F. Busnengo, A. Salin and W. Dong, *J. Chem. Phys.*, 2000, **112**, 7641–7651.

(157) C. Díaz, R. A. Olsen, H. F. Busnengo and G.-J. Kroes, *J. Phys. Chem. C*, 2010, **114**, 11192–11201.

(158) J. Ischtwan and M. A. Collins, *J. Chem. Phys.*, 1994, **100**, 8080–8088.

(159) M. A. Collins, *Theor. Chem. Acc.*, 2002, **108**, 313–324.

(160) J. Behler, *Phys. Chem. Chem. Phys.*, 2011, **13**, 17930–17955.

(161) S. Manzhos, X. Wang, R. Dawes and T. Carrington, *J. Phys. Chem. A*, 2006, **110**, 5295–5304.

(162) B. J. Braams and J. M. Bowman, *Int. Rev. Phys. Chem.*, 2009, **28**, 577–606.

(163) B. Jiang and H. Guo, *J. Chem. Phys.*, 2013, **139**, 054112.

(164) B. Jiang and H. Guo, *J. Chem. Phys.*, 2014, **141**, 034109.

(165) K. Hermann, *Crystallography and Surface Structure: An Introduction for Surface Scientists and Nanoscientists*, John Wiley & Sons, 2011.

(166) N. Materer, A. Barbieri, D. Gardin, U. Starke, J. D. Batteas, M. A. Van Hove and G. A. Somorjai, *Phys. Rev. B*, 1993, **48**, 2859.

(167) R. Baer and R. Kosloff, *J. Chem. Phys.*, 1997, **106**, 8862–8875.

(168) C. P. Koch, T. Klüner, H.-J. Freund and R. Kosloff, *J. Chem. Phys.*, 2003, **119**, 1750–1765.

(169) D. Gelman and R. Kosloff, *Chem. Phys. Lett.*, 2003, **381**, 129–138.

(170) H. Wang and M. Thoss, *J. Chem. Phys.*, 2003, **119**, 1289–1299.

(171) U. Manthe, *J. Chem. Phys.*, 2008, **128**, 164116.

(172) H. Wang, *J. Phys. Chem. A*, 2015, **119**, 7951–7965.

(173) M. Nest and P. Saalfrank, *J. Chem. Phys.*, 2000, **113**, 8753–8761.

(174) J. C. Tremblay and P. Saalfrank, *J. Chem. Phys.*, 2009, **131**, 084716:1–17.

(175) J. C. Tremblay, G. Füchsel and P. Saalfrank, *Phys. Rev. B*, 2012, **86**, 045438.

(176) H.-P. Breuer, W. Huber and F. Petruccione, *Comput. Phys. Commun.*, 1997, **104**, 46–58.

(177) P. Saalfrank, *Chem. Phys.*, 1996, **211**, 265–276.

(178) D. E. Manolopoulos, *J. Chem. Phys.*, 2002, **117**, 9552–9559.

(179) N. Lorente and H. Ueba, *Eur. Phys. J. D.*, 2005, **35**, 341–348.

(180) B. Hellsing and M. Persson, *Phys. Scr.*, 1984, **29**, 360.

(181) T. Liu, B. Fu and D. H. Zhang, *J. Chem. Phys.*, 2013, **139**, 184705.

(182) T. Liu, B. Fu and D. H. Zhang, *J. Chem. Phys.*, 2014, **140**, 144701.

(183) T. Liu, B. Fu and D. H. Zhang, *J. Chem. Phys.*, 2014, **141**, 194302.

(184) T. Liu, Z. Zhang, B. Fu, X. Yang and D. H. Zhang, *Chem. Sci.*, 2016, **7**, 1840–1845.

(185) G.-J. Kroes and C. Díaz, *Chem. Soc. Rev.*, 2016, **45**, 3658–3700.

(186) E. Pijper, M. F. Somers, G.-J. Kroes, R. A. Olsen, E. J. Baerends, H. F. Busnengo, A. Salin and D. Lemoine, *Chem. Phys. Lett.*, 2001, **347**, 277–284.

(187) C. Díaz, E. Pijper, R. A. Olsen, H. F. Busnengo, D. J. Auerbach and G.-J. Kroes, *Science*, 2009, **326**, 832–834.

(188) G. Füchsel, S. Schimka and P. Saalfrank, *J. Phys. Chem. A*, 2013, **117**, 8761–8769.

Danksagung

Zum Abschluss dieser Dissertation möchte ich einigen Menschen danken, die durch ihre Unterstützung auf verschiedenen Ebenen zum Gelingen dieser Arbeit beigetragen haben.
Mein erster Dank geht dabei an Jean Christophe Tremblay. Mit deiner begeisternden Art standest du mir bei Fragen und Problemen stets mit Rat und Tat zur Seite. Unsere zahlreichen Diskussionen haben mich viel gelehrt und meinen wissenschaftlichen Horizont erweitert. Du bist ein Doktorvater, wie man ihn sich besser nicht wünschen kann.
Ein weiterer Dank geht an Beate Paulus, nicht nur für ihre wissenschaftliche und organisatorische Unterstützung seit der Bachelorarbeit, sondern auch für die Möglichkeit in der Lehre tätig zu sein. Die dabei erlangten Erfahrungen sind ein wertvoller Pfeiler meiner wissenschaftlichen Entwicklung.
Dr. Gernot Füchsel möchte ich für die wissenschaftliche Kooperation während des letzten Teils dieser Dissertation danken. Allen aktiven und ehemaligen Mitgliedern der Arbeitsgruppen der Theoretischen Chemie danke ich für das angenehme Arbeitsklima. Ein besonderer Dank gebührt dabei meinem langjährigen Büropartner Frederik Bader für die unzähligen wissenschaftlichen und nichtwissenschaftlichen Diskussionen, sowie das tapfere Erdulden meiner mittäglichen Monologe.
Dem Land Berlin danke ich für die finanzielle Unterstützung durch das Elsa-Neumann-Stipendium.
Der größte Dank gilt meiner Familie, insbesondere meinen Eltern, die all die Jahre durch ihre uneingeschränkte Unterstützung meinen Werdegang überhaupt erst ermöglicht haben.